Recent Advances in Mathematics-II

EDITOR
Assist. Prof. Dr. Esen HANAÇ DURUK

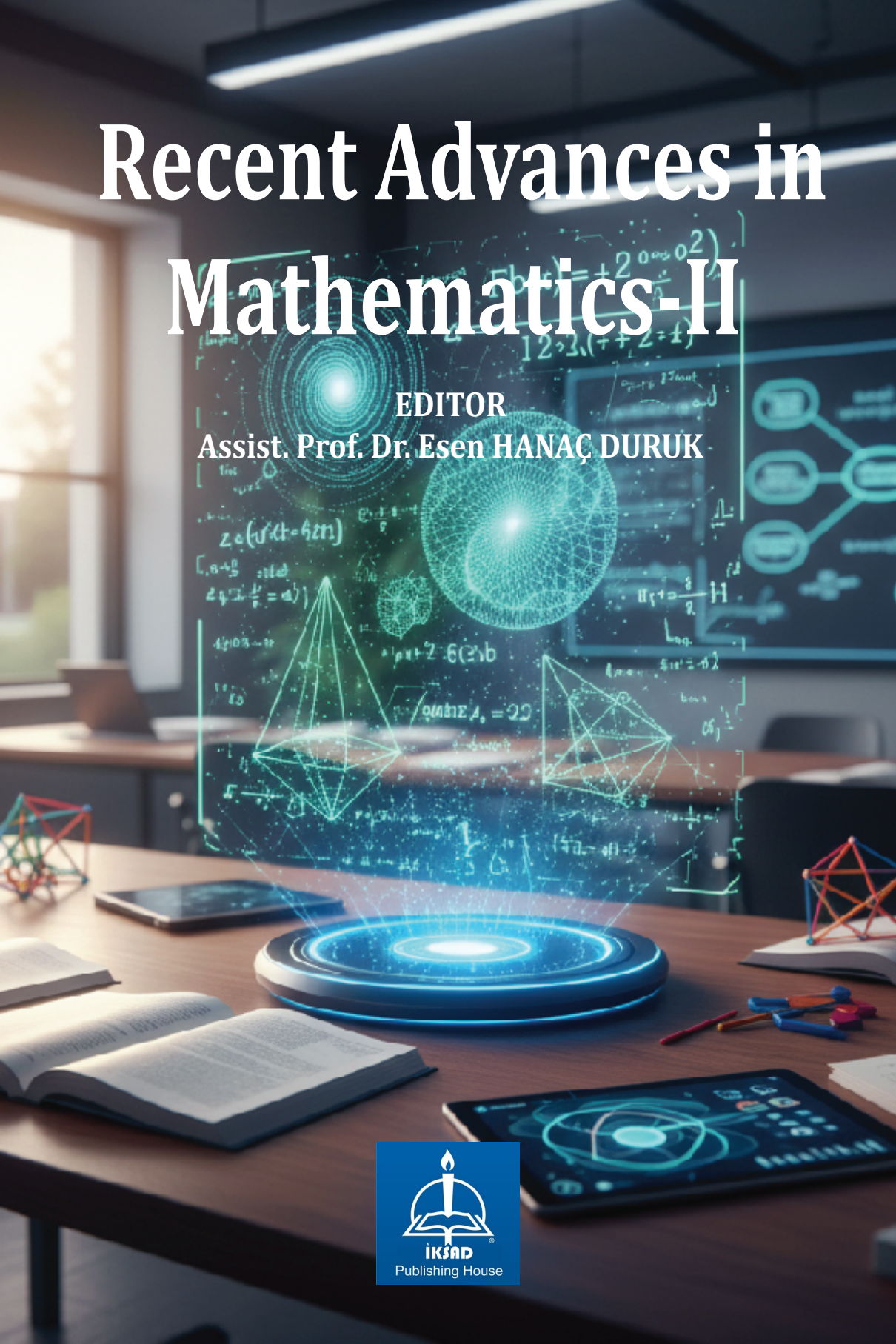

İKSAD
Publishing House

RECENT ADVANCES IN MATHEMATICS-II

EDITOR

Assist. Prof. Dr. Esen HANAÇ DURUK

AUTHORS

Assoc. Prof. Dr. Kadir Can ERBAŞ

Assoc. Prof. Dr. Kübra GÜL

Assoc. Prof. Dr. Levent ÖZBEK

Assoc. Prof. Dr. Yeşim AKÜZÜM ÖZEN

İKSAD
Publishing House

(The Licence Number of Publicator: 2014/31220)
TÜRKİYE TR: +90 342 606 06 75
USA: +1 631 685 0 853
E mail: iksadyayinevi@gmail.com
www.iksadyayinevi.com

It is responsibility of the author to abide by the publishing ethics rules.
Iksad Publications – 2025©

ISBN: 978-625-378-456-0
Cover Design: İbrahim KAYA
December / 2025
Ankara / Türkiye
Size: 16x24cm

CONTENTS

PREFACE

Our book is titled Recent Advances in Mathematics-II. The book primarily discusses the new methodologies, including identifying and building three-fold orthogonal systems, making important contributions to differential geometry's theoretical and practical features, the matrix-based techniques employed here may be applied to similar algebraic systems, the compartmental model was assessed using experimental data that partners supplied, the Kalman-based models for sophisticated avian species growth analysis and the Hadamard-type Pell-p sequence is extended to groups by introducing the Hadamard-type Pell-p orbit and redefining it using group elements. There are certain methods for summarizing the problems that make the concepts clear in each chapter. It is envisaged that the book will meet the demands of researchers from a variety of professional sectors because each topic is addressed with care. Thus, the research in this topic is quite important and useful for their specific interests. I want to express my gratitude to the writers for their priceless contributions and the publishing house for their assistance.

Assist. Prof. Dr. Esen HANAÇ DURUK

CHAPTER 1

EXISTENCE AND DISCOVERY OF TRIPLY ORTHOGONAL LEVEL OR PARAMETRIC SURFACES

Assoc. Prof. Dr. Kadir Can ERBAŞ[1]

DOI: https://www.doi.org/10.5281/zenodo.18077698

[1] Başkent University, Faculty of Engineering, Department of Biomedical Engineering, Ankara, Türkiye. kcerbas@gmail.com, orcid id: 0000-0002-6446-829X

1. INTRODUCTION

Triple orthogonal coordinate systems are one of the fundamental structures in mathematical physics, differential geometry and applied sciences. These systems provide a special coordinate structure, each point of which is uniquely defined by a family of three orthogonal surfaces (Weatherburn, 1926; Eisenhart, 1907; Kasner, 1911; Zund & Moore 1987; Wright, 1906). These systems, which treat linear and surface structures orthogonally, have been frequently used to solve mathematical and physical problems. Developed in the 18th century by Leibniz and Euler, canonical coordinates played a fundamental role in the evaluation of multiple integrals and evolved in the light of triple orthogonal systems (Bobenko, 2003). In the 19th century, mathematicians such as Gabriel Lamé and Gaston Darboux generalized these systems and made them a fundamental element of differential geometry. Important geometric principles such as Dupin's theorem paved the way for triply orthogonal systems in both mathematical and physical terms and laid the foundation for important applications in modern science (Zakharov, 1998).

These systems are characterized by the existence of three different families of orthogonal intersecting surfaces at each point in space (Garcia & Tejada, 2023). This orthogonal structure of surface families offers an impressive range of solutions in both theoretical and practical applications. For example, while the Cartesian coordinate system provides a simple example with orthogonal plane families, more complex systems such as homofocal quadrics or ellipsoidal coordinates can be adapted to different geometric and physical problems. The order offered by these systems has played a critical role in solving differential equations, applying boundary conditions and modeling physical phenomena (Ferréol, 2017).

The development of triply orthogonal systems has been closely related to the historical progress of differential geometry (Bobenko, 2003). Dupin's theorem, proved by Charles Dupin in 1813, established the basic geometric properties of triply orthogonal systems. This theorem guarantees that the intersection points of three different families of surfaces are perpendicular to the lines on each surface. Following Dupin's work, Gabriel Lamé developed the mathematical theory of these systems and showed their applicability to physical problems. Gaston Darboux extended Lamé's work and applied many fundamental concepts of differential geometry to these systems and laid an

important foundation for modern mathematical physics (Colapinto, 2017;Colapinto, 2017;Smith, 2004).

One of the important features of these systems is that they can be defined based on a Jacobian matrix. The system satisfies the condition that the columns of the matrix are orthogonal to each other (Abdelmagid et al., 2023; Finat, 2018). Moreover, the fact that these systems can be preserved by various transformations, e.g., inversion transformations or Bianchi and Bäcklund transformations, provides an important advantage, especially in theoretical physics and mathematics (Eisenhart, 1907). The Cayley-Darboux equation provides critical information about the existence and properties of these systems and is an important part of understanding the complex structures of differential geometry.

The importance of triple orthogonal coordinate systems in modern science stems from their applicability to various physical and mathematical problems. In areas such as the propagation of light waves, the calculation of electromagnetic fields and fluid mechanics, triple orthogonal systems provide efficient solutions in different geometries (Ryskin & Leal, 1983; Sizykh, 2020; Lester et al., 2022; Panou, 2014). With a wide range of applications ranging from geodetic problems to architectural design, these systems are an important component of scientific innovation. Ellipsoidal coordinate systems are frequently used in surface geodetic analysis to calculate the Earth's gravitational potential (Panou, 2014). In architecture, these systems allow complex geometries to be more easily analyzed and optimized. By combining aesthetics and structural durability, it paves the way for new designs in architecture and engineering (Abdelmagid et al.,2022).

Triple orthogonal coordinate systems have a wide scope from differential geometry to numerical methods. The easier application of boundary conditions, the creation of numerical meshes suitable for complex geometries and the improvement of solution accuracy are the distinguishing features of these systems. In numerical techniques such as the finite element method, the regularization and simplification possibilities offered by these systems have increased solution productivity in modern computational applications (Panou, Korakitis & Delikaraoglou, 2016).

Although the debate on this topic dates back more than 100 years, mathematical research and its applications in engineering have been explored

in recent years. Research in mathematics and differential geometry has taken a modern form with the development of computer technology. Menjanahary et al. investigate Dupin cyclic cubes, and their singularities using orthogonal coordinate systems and classify them according to Möbius equivalence in Euclidean space. These cubes are derived from triple orthogonal coordinate systems in which all coordinate lines are circles or straight lines (Menjanahary, Hoxhaj & Krasauskas, 2024). Hoque et al. investigated the second-order integrability of systems with velocity-dependent potential in three-dimensional Euclidean space. They utilized various orthogonal coordinate systems such as elliptic cylindrical, prolate/oblate spheroidal and circular parabolic coordinate systems (Hoque et al., 2023). Strunz successfully derived unit vector transformations between Cartesian and SOS coordinate systems. The SOS coordinate system is a powerful tool that can simplify the solution of problems exhibiting oblate spheroid geometry. It can be used to model and analyze physical phenomena that exhibit oblate spheroid geometry, especially in fields such as astrophysics and geophysics (Strunz, 2023).

In particular, the transformation of orthogonal coordinate systems is common in solving problems in fluid mechanics. Viaggiu presents an algorithm for generating anisotropic fluids with or without heat flow but with vanishing viscosity, starting from general stationary axisymmetric space-times connected to two spatially isotropic orthogonal coordinates (Viaggiu, 2018). Ivers studies the dynamo effect created by the motion of a conducting fluid in an oblate spheroidal volume. His work addresses the kinematic dynamo problem, which is important for understanding how the magnetic field is generated and maintained and presents an innovative method for obtaining numerical solutions in oblate spheroid geometries. In summary, Ivers uses homoeoidal oblate spheroidal coordinate systems to model complex magnetic fields and fluid motions (Ivers, 2017). Hester and Vasil develop a coordinate system for understanding regions around changing smooth surfaces and curves. In particular, it makes use of the signed-distance function, as implemented in the level set and related methods. This work is believed to present the first comprehensive fundamental derivation of a complete vector calculus for this orthogonal coordinate system. This is necessary to define the vector Laplacian, or advective derivative, which commonly arises in boundary layer calculations

in fluid mechanics. This method uses orthogonal coordinates to define points near surfaces and curves (Hester & Vasil, 2023).

There are also important studies in electrical engineering. Malits et al. studied TEM mode wave propagation in a microstrip transmission line on a dielectric substrate with a circular segment cross section. The proposed microstrip design is suitable for fabrication and allows miniaturization of the microstrip since there is no lateral fringing effect of the substrate in the transmitted fundamental TEM mode. The authors used the bipolar orthogonal coordinate system to reformulate the problem in the form of trigonometric double integral equations (Malits, Haridim & Chulski, 2015). Kubu et al. consider integrable and super integrable systems with second-order integrals of motion moving in the presence of a magnetic field in three-dimensional Euclidean space. They find that the system in question is a system involving a magnetic field and is minimally super integrable. They also report that this system cannot be separated in any orthogonal coordinate system. This means that the Hamilton-Jacobi equation of the system cannot be solved by separation of variables in any known orthogonal coordinate system, such as Cartesian, cylindrical or spherical coordinates (Kubů, Marchesiello & Šnobl, 2023).

Orthogonal coordinate systems are also utilized in industrial and aeronautical engineering. Bae and Choi focus on NURBS surface fitting using orthogonal coordinate transformation to speed up product development processes and propose a method for precise and efficient modeling of complex freeform surfaces (Bae & Choi, 2002). A computer graphics program called Spacebar, a tool developed to facilitate the design and analysis of lightweight kinematic mechanisms such as aircraft control systems, landing gears and door hinges, is reported by Ricci to generate geometric positioning data in orthogonal coordinates (x, y, z) of the mechanism model. It is also explained that the program assumes that the applied loads are applied along the basic x, y, z orthogonal axis of the mechanism (Ricci, 1976).

In the future, triply orthogonal coordinate systems are expected to increase their applicability in solving more complex problems and in new scientific fields. These systems will continue to make critical contributions to the advancement of modern science and technology with their advantages in both theoretical and practical applications.

At the end of the 19th and the beginning of the 20th century, the topic of triply orthogonal surface families was investigated by important mathematicians such as Weatherburn (Weatherburn, 1926), Eisenhart (Eisenhart, 1907), Kasner (Kasner, 1911; Kasner, 1909), Wright (Wright, 1906), Darboux (Darboux, 1910), Cayley (Cayley, 1872; Cayley, 1873), Hotine (Hotine, 1966), etc., but afterwards the interest in this topic declined. These researchers generally focused a lot on the existence and properties of families of triple orthogonal surfaces, but they did not provide enough information on practical applications and how to obtain coordinate systems. The lack of computer technology at the time explains the absence of practical research on this topic.

This paper introduces a different approach for investigating the existence of triple orthogonal systems without requiring advanced knowledge of differential geometry. It addresses the challenge of identifying two surface families orthogonal to a given surface family and to each other, providing a detailed explanation of the methodology. Additionally, for surface families expressed in closed form, a MATLAB script has been developed to compute and list the corresponding results. This practical approach is designed to appeal to researchers in diverse fields, including cartographic engineering, astrophysics, electromagnetism, fluid mechanics, and boundary value problems.

2. FAMILIES OF TRIPLY ORTHOGONAL LEVEL SURFACES (TOLS)

In this section, it would be appropriate to first mention the terminology. The keywords frequently used in the literature are "triply orthogonal system", "triply orthogonal coordinates", "triply orthogonal coordinate system", "triply orthogonal families", "triply orthogonal families of surfaces" and "triply orthogonal surface". The system or coordinate system referred to in these terms refers to a coordinate system of triply orthogonal surfaces. To be a coordinate system, just as in spherical and cylindrical coordinates, the functions describing the surfaces must be expressed as level surfaces, that is, as implicit functions. The term "triply orthogonal level surfaces" (TOLS) will be used in this paper to refer to the triply orthogonal systems that satisfy this condition, i.e. the families of surfaces referred to in the literature as triply orthogonal systems.

The term "triply orthogonal parametric surface" (TOPS) is appropriate for families of orthogonal surfaces that cannot be expressed as level surfaces without such a condition.

2.1 Definition of the Problem

$$f(x,y,z) = U \quad (1)$$

$$g(x,y,z) = V, \qquad h(x,y,z) = W \quad (2)$$

$$\vec{\nabla} f \cdot \vec{\nabla} g = \vec{\nabla} f \cdot \vec{\nabla} h = \vec{\nabla} h \cdot \vec{\nabla} g = 0 \quad (3)$$

Given a family of level surfaces described by Eq. (1), is it possible to identify two additional families of level surfaces that are orthogonal to this surface family and to each other? Specifically, do there exist functions g and h such that the conditions in Eq. (2) and Eq. (3) are satisfied?

2.2 General Solution Method of the Problem

To simplify the solution of the problem, let us consider the vector functions K, L, M obtained by multiplying the gradients of the functions *f, g,* and *h* by scalar functions S_1, S_2, and S_3. These vectors will be parallel to the gradients of the functions.

$$\vec{K}(x,y,z) = \big(K_1(x,y,z), K_2(x,y,z), K_3(x,y,z)\big) = S_1(x,y,z)\vec{\nabla} f(x,y,z) \quad (4)$$

$$\vec{L}(x,y,z) = \big(L_1(x,y,z), L_2(x,y,z), L_3(x,y,z)\big) = S_2(x,y,z)\vec{\nabla} g(x,y,z) \quad (5)$$

$$\vec{M}(x,y,z) = \big(M_1(x,y,z), M_2(x,y,z), M_3(x,y,z)\big) = S_3(x,y,z)\vec{\nabla} h(x,y,z) \quad (6)$$

To hold Eq.3

$$\vec{K} \cdot \vec{L} = K_1 L_1 + K_2 L_2 + K_3 L_3 = 0 \quad (7)$$

$$\vec{M} = \vec{K} \times \vec{L} \quad (8)$$

must be satisfied. For an arbitrary function *T(x,y,z),*

$$\vec{L} = (K_2, -K_1 - K_3 T, K_2 T) \quad (9)$$

can be written because the dot product of this vector with K will be zero for every value of *T*. After the cross product,

$$\vec{M} = (K_1K_3 + (K_2^2 + K_3^2)T, K_2K_3 - K_1K_2T, -(K_1^2 + K_2^2) - K_1K_3T) \quad (10)$$

is obtained. The function T can be defined as the tangent of the angle with the $+x$ axis of the projection of the gradient of g in the xz plane.

Since the functions K_1, K_2, and K_3 are known from the given function f, the vectors L and M depend on the only unknown function T. Given any function T, Eq.11 is satisfied but it is not obvious that the vectors L and M are gradients of scalar functions.

$$\vec{K} \perp \vec{L} \perp \vec{M} \quad (11)$$

2.3 A Vector as a Gradient of a Scalar Function

The basic problem here is whether a given vector L, when multiplied by a suitable scalar function S, will be a gradient of another scalar function. Since the curl of gradient of a scalar function is zero, vector L and scalar S must satisfy Eq.12.

$$\vec{\nabla} \times (S\vec{\mathrm{L}}) = 0 \quad (12)$$

Applying the multiplication rule for derivatives gives

$$\vec{\nabla}S \times \vec{\mathrm{L}} + S\,\vec{\nabla} \times \vec{\mathrm{L}} = 0. \quad (13)$$

After some algebra, Eq.14 is obtained.

$$-\frac{\vec{\nabla}S}{S} \times \vec{\mathrm{L}} = \vec{\nabla} \times \vec{\mathrm{L}} \rightarrow \quad \vec{\nabla} \times \vec{\mathrm{L}} = \vec{\nabla}(-\ln S) \times \vec{\mathrm{L}} \quad (14)$$

If the dot product of both sides of Eq.14 with the vector L is taken, Equation 15 is obtained.

$$\vec{\mathrm{L}} \cdot \vec{\nabla} \times \vec{\mathrm{L}} = \vec{\mathrm{L}} \cdot \vec{\nabla}(-\ln S) \times \vec{\mathrm{L}} \quad (15)$$

Since the right side of Eq.15 will be zero because of vector algebraic rules, Eq.16 is valid.

$$\vec{\mathrm{L}} \cdot \vec{\nabla} \times \vec{\mathrm{L}} = 0 \quad (16)$$

Eq.16 must be satisfied so that when vector L is multiplied by a suitable scalar, it can be written as the gradient of a scalar function. The expression on the left-hand side of Eq.16 is known as the *helicity density* of the vector L.

2.4 Key to Solving the Problem

The vectors we must express as gradients are the vectors in Eq. 9 and 10, so they must satisfy Equation 16. From this, Eq.17-18 is written.

$$\vec{L} \cdot \vec{\nabla} \times \vec{L} = 0 \quad (17)$$

$$\vec{M} \cdot \vec{\nabla} \times \vec{M} = 0 \quad (18)$$

When Eqs.17-18 are expanded, Eqs.19-20 are obtained, which are the equations that function T must satisfy. The subscripts x, y, z denote partial derivative.

$$L_1(L_{3y} - L_{2z}) + L_2(L_{1z} - L_{3x}) + L_3(L_{2x} - L_{1y}) = 0 \quad (19)$$

$$M_1(M_{3y} - M_{2z}) + M_2(M_{1z} - M_{3x}) + M_3(M_{2x} - M_{1y}) = 0 \quad (20)$$

The arrangement of Eq.17-20 in terms of T is shown in Eq.21-28.

$$\vec{L} = (K_2, -K_1, 0) + (0, -K_3, K_2)T \quad (21)$$

$$\vec{M} = (K_1K_3, K_2K_3, -K_1^2 - K_2^2) + (K_2^2 + K_3^2, -K_1K_2, -K_1K_3)T \quad (22)$$

$$\vec{\lambda} = (K_2, -K_1, 0), \qquad \vec{l} = (0, -K_3, K_2) \rightarrow \ \vec{L} = \vec{\lambda} + \vec{l}T \quad (23)$$

$$\vec{\mu} = (K_1K_3, K_2K_3, -K_1^2 - K_2^2), \qquad \vec{m} = (K_2^2 + K_3^2, -K_1K_2, -K_1K_3) \rightarrow \ \vec{M} = \vec{\mu} + \vec{m}T \quad (24)$$

$$\vec{L} \cdot \vec{\nabla} \times \vec{L} = (\vec{\lambda} + \vec{l}T) \cdot \nabla \times (\vec{\lambda} + \vec{l}T) = (\vec{\lambda} + \vec{l}T) \cdot \left((\nabla \times \vec{\lambda} + T\vec{\nabla} \times \vec{l} + \vec{\nabla}T \times \vec{l})\right) = 0 \quad (25)$$

$$\vec{\lambda} \cdot \nabla \times \vec{\lambda} + T(\vec{l} \cdot \nabla \times \vec{\lambda} + \vec{\lambda} \cdot \vec{\nabla} \times \vec{l}) + T^2\vec{l} \cdot \vec{\nabla} \times \vec{l} + \vec{\lambda} \cdot \vec{\nabla}T \times \vec{l} + T\vec{l} \cdot \vec{\nabla}T \times \vec{l} = 0 \quad (26)$$

In Eq.26, the identities of $\vec{\lambda} \cdot \vec{\nabla}T \times \vec{l} = \vec{\nabla}T \cdot \vec{l} \times \vec{\lambda}$ and $\vec{l} \cdot \vec{\nabla}T \times \vec{l} = 0$ are substituted so it is simplified. In addition, $\vec{l} \times \vec{\lambda} = K_2\vec{K}$ is considered. Thus,

$$K_2\vec{K} \cdot \vec{\nabla}T + T^2\vec{l} \cdot \vec{\nabla} \times \vec{l} + (\vec{l} \cdot \nabla \times \vec{\lambda} + \vec{\lambda} \cdot \vec{\nabla} \times \vec{l})T + \vec{\lambda} \cdot \nabla \times \vec{\lambda} = 0 \quad (27)$$

is obtained. Similarly, the equation of $\vec{m} \times \vec{\mu} = K_2(K_1^2 + K_2^2 + K_3^2)\vec{K}$ must be considered. Finaly, Eq.28 is obtained

$$K_2(K_1^2+K_2^2+K_3^2)\vec{K}\cdot\vec{\nabla}T+\vec{m}\cdot\vec{\nabla}\times\vec{m}T^2+\\(\vec{m}\cdot\nabla\times\vec{\mu}+\vec{\mu}\cdot\vec{\nabla}\times\vec{m})T+\vec{\mu}\cdot\nabla\times\vec{\mu}=0 \quad (28)$$

To make Eq.27 similar to Eq.28, multiply both sides of Eq.27 by $(K_1^2+K_2^2+K_3^2)$.

$$K_2(K_1^2+K_2^2+K_3^2)\vec{K}\cdot\vec{\nabla}T+\vec{l}\cdot\vec{\nabla}\times\vec{l}(K_1^2+K_2^2+K_3^2)T^2+\\(\vec{l}\cdot\nabla\times\vec{\lambda}+\vec{\lambda}\cdot\vec{\nabla}\times\vec{l})(K_1^2+K_2^2+K_3^2)T+\vec{\lambda}\cdot\nabla\times\vec{\lambda}(K_1^2+K_2^2+K_3^2)=0 \quad (29)$$

In Eqs. 28 and 29, all expressions except *T* are known in terms of partial derivatives of *f(x,y,z)*. To find the function *T* satisfying Equations 28 and 29, the coefficients of *T* are named as in Eqs.30-31 and finally written as in Equations 32-33.

$$A_1=(K_1^2+K_2^2+K_3^2)\vec{l}\cdot\vec{\nabla}\times\vec{l}\\B_1=(K_1^2+K_2^2+K_3^2)(\vec{l}\cdot\nabla\times\vec{\lambda}+\vec{\lambda}\cdot\vec{\nabla}\times\vec{l}) \quad (30)\\C_1=(K_1^2+K_2^2+K_3^2)\vec{\lambda}\cdot\nabla\times\vec{\lambda}$$

$$A_2=\vec{m}\cdot\vec{\nabla}\times\vec{m}\\B_2=(\vec{m}\cdot\nabla\times\vec{\mu}+\vec{\mu}\cdot\vec{\nabla}\times\vec{m}) \quad (31)\\C_2=\vec{\mu}\cdot\nabla\times\vec{\mu}$$

$$K_2(K_1^2+K_2^2+K_3^2)\vec{K}\cdot\vec{\nabla}T+A_1T^2+B_1T+C_1=0\\K_2(K_1^2+K_2^2+K_3^2)\vec{K}\cdot\vec{\nabla}T+A_2T^2+B_2T+C_2=0 \quad (32)$$

Since the first terms of Eq.32 are equal, the other terms must also be equal (Eq.33).

$$A_1T^2+B_1T+C_1=A_2T^2+B_2T+C_2\\(A_1-A_2)T^2+(B_1-B_2)T+C_1-C_2=0 \quad (33)$$

If function *T* found from Eq.33 also satisfies Eq.32, then the *T* function we are looking for is found. A MATLAB code that performs these complicated operations is given in Appendix A. Once the T function is found, an integral

multiplier must be found to make the L and M vectors the gradient of g and h (Eq.34).

$$\begin{matrix}\vec{\nabla}g = \varphi(x,y,z)\vec{L}, \\ \vec{\nabla}h = \psi(x,y,z)\vec{M}\end{matrix} \quad (34)$$

2.5 Solution of *g(x,y,z)* and *h(x,y,z)*

To find the function g from Eq.34, the expansion of this equation is written in Eq.35. To eliminate the function φ, which is the integral multiplier in Eq.35, Eq.36 is written.

$$\begin{matrix}g_x = \varphi L_1 \\ g_y = \varphi L_2 \\ g_z = \varphi L_3\end{matrix} \quad (35)$$

$$L_2 g_x - L_1 g_y = 0, \qquad L_3 g_x - L_1 g_z = 0, \qquad L_3 g_y - L_2 g_z = 0, \quad (36)$$

The main objective is to find any special solution g that satisfies all three equations in Eq.36. For this purpose, a characteristic curve equation can be written for the partial differential equations in Eq.36 and the simplest special solution can be tried for all three. The solution of the characteristic equations will be found from Eq.37.

$$\frac{dy}{dx} = -\frac{L_1}{L_2}, \qquad \frac{dz}{dx} = -\frac{L_1}{L_3}, \qquad \frac{dz}{dy} = -\frac{L_2}{L_3}. \quad (37)$$

Closed solutions of the form $F_i(x,y,z) = c$ to be obtained from the solution of the equation in Eq.37 can be used as the *g(x,y,z)* we are looking for.

Example 1: Find the triple orthogonal level surfaces (TOLS) to the surface family $f(x,y,x) = x^2 + y^2 + 2z^2 = U$.

Solution 1: The level surface term means that the three mutually perpendicular surfaces must be written in closed form, i.e. as in Eq.2. For this, the function T in Eq.32-33 needs to be found. When the MATLAB script in Appendix A is run, two T functions for the function f here appear: $T = 0, or\ T = -(x^2 + y^2)/2xz$. For these T values, vectors L and M are found in Eq.38.

$$\begin{aligned} T = 0 \rightarrow \quad & \vec{L} = (y, -x, 0), \qquad \vec{M} = (2xz, 2yz, -x^2 - y^2), \\ T = -\frac{(x^2 + y^2)}{2xz} \rightarrow \quad & \vec{L} = (2xz, 2yz, -x^2 - y^2), \qquad \vec{M} = (y, -x, 0). \end{aligned} \tag{38}$$

Notice that if two different solutions are found and then substituted in Eq.21-21, we get two symmetric solutions as in Eq.34. This is natural because there must be two vectors perpendicular to *grad(f)* in space. Therefore, it is sufficient to use one of the two solutions of T. For the solution method described in section 2.5, the first of the equations in Eq.37 is written for the vectors *L* and *M* in Eq.38 and its solution is found as in Eq.39

$$\frac{dy}{dx} = \frac{y}{x} \rightarrow \frac{y}{x} = c_1(z), \qquad g(x, y, z) = \frac{y}{x}. \tag{39}$$

The gradient of *g* from Eq.39 is indeed parallel to vector *L*. Then *g(x,y,z)* is found. Similarly, Eq.40 is written for *M*.

$$\frac{dy}{dx} = -\frac{x}{y} \rightarrow x^2 + y^2 = c_2(z), \qquad \frac{dz}{dx} = \frac{2xz}{x^2 + y^2} \rightarrow \frac{x^2 + y^2}{z} = c_3(y). \tag{40}$$

The gradient of the function with integral constant $c_3(y)$ is parallel to the vector *M*, so this is the appropriate function *h*. In summary, the functions *g* and *h* appear in Eq.41.

$$g(x, y, z) = \frac{y}{x}, \qquad h(x, y, z) = \frac{x^2 + y^2}{z}. \tag{41}$$

As a result, the triple orthogonal system we found in this example is given in Eq.42.

$$x^2 + y^2 + 2z^2 = U, \qquad \frac{y}{x} = V, \qquad \frac{x^2 + y^2}{z} = W. \tag{42}$$

These surfaces are shown in Figure 1 for any starting point x_0,y_0,z_0. To obtain the coordinate surfaces by changing the starting point, you can access the simulation prepared in Desmos.com from this link (https://www.desmos.com/3d/pw3ge8ztwp). The solution in Eq.42 can be checked by Appendix C typing the corresponding functions *f, g* and *h* .

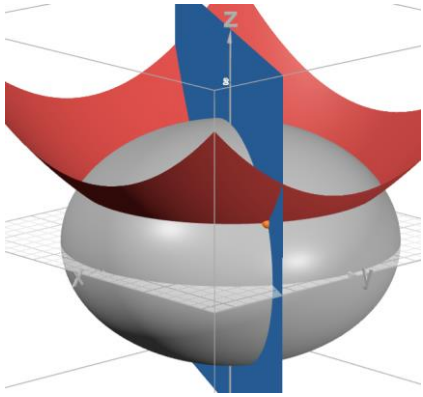

Fig.1: Surface families for Example 1.

Example 2:

Find the triple orthogonal coordinate surfaces to the surface family $f(x,y,x) = x^2 + y^2 + z^2 = U$.

Solution 2.a:

The family of reference surfaces given in this example are spheres with the origin at the center. When the script in Appendix A is run for $f = x^2 + y^2 + z^2$, it is seen that all 6 coefficients A, B, C in Equation 32 are zero. In this case, there will be infinite function T satisfying the equation $\vec{K} \cdot \vec{\nabla} T = 0$. That is, for each value of T satisfying the equation $xT_x + yT_y + zT_z = 0$, there will be a set of vectors L and M. All functions of the form $T = F\left(\frac{y}{x}, \frac{xy}{z^2}\right)$ are solutions. Vectors *L* and *M* for *T=0*, which is one of the *T* values satisfying this equation, are shown in Equation 43.

$$T = 0 \rightarrow \qquad \vec{L} = (y, -x, 0), \quad \vec{M} = (xz, yz, -x^2 - y^2), \tag{43}$$

The vectors *L* and *M* can be the gradient of the functions *g* and *h* when divided by $-xy$ and $z(x^2 + y^2)$ respectively (Equation 44).

$$\vec{\nabla} g = -\frac{1}{xy}\vec{L} = \left(-\frac{1}{x}, \frac{1}{y}, 0\right), \quad \vec{\nabla} h = \frac{1}{z(x^2 + y^2)}\vec{M} = \left(\frac{x}{(x^2 + y^2)}, \frac{y}{z(x^2 + y^2)}, -\frac{1}{z}\right), \tag{44}$$

Eq.44 yields the functions g and h as follows, which are the famous spherical coordinates.

$$g = \frac{y}{x} = V = \tan\varphi\,, \qquad h = \frac{x^2+y^2}{z^2} = W = \tan^2\theta. \tag{45}$$

In Solution 2.a, the method described in Section 2.5 could also be used. For example, if $dz/dx = xz/(x^2+y^2)$, the function h will be found in the same way. The choice of such different solutions is left to the reader. If the given surface family is a surface of revolution, one can practically find families of triple orthogonal surfaces. This is explained in Appendix B. Since the surface family here is a surface of revolution family, readers may also refer to the procedure described in Appendix B.

Solution 2.b:

An infinite coordinate system can be written for this example. For example, if the function T is assigned as a constant at a value such as T=p, vectors L and M are obtained as follows.

$$\vec{L} = (y, -x-pz, py), \qquad \vec{M} = (py^2+pz^2+xz, y(z-px), -x^2-pzx-y^2), \tag{46}$$

Integral factors for *L* and *M:*

$$\vec{\nabla}g = \frac{1}{y^2}\vec{L} = \left(\frac{1}{y}, -\frac{x+pz}{y^2}, \frac{p}{y}\right), \qquad \vec{\nabla}h = \frac{1}{(px-z)^3}\vec{M} = \left(\frac{py^2+pz^2+xz}{(px-z)^3}, \frac{y(z-px)}{(px-z)^3}, -\frac{x^2+pzx+y^2}{(px-z)^3}\right), \tag{47}$$

$$g = \frac{y}{x+pz} = V, \qquad h = \frac{x^2+y^2+z^2}{(z-px)^2} = W \tag{48}$$

The functions *f(x,y,z)* in Example 2 and g and h in Eq.48 form an alternative spherical coordinate system. Click here to see this system in 3D.

Solution 2.c:

$$T = \frac{y^2}{xz} \rightarrow \qquad \vec{L} = (xyz, -z(x^2+y^2), y^3), \qquad \vec{M} = \left(x^2z^2+y^4+y^2z^2, -xy(y^2-z^2), -xz(x^2+2y^2)\right), \tag{49}$$

Integral factors for *L* and *M*

$$\vec{\nabla} g = \frac{1}{y^3 z}\vec{L} = \left(\frac{x}{y^2}, -\frac{(x^2+y^2)}{y^3}, \frac{1}{z}\right),$$

$$\vec{\nabla} h = \frac{1}{x^2(x^2+2y^2)^{\frac{3}{2}}}\vec{M} = \begin{pmatrix} \frac{x^2z^2+y^4+y^2z^2}{x^2(x^2+2y^2)^{\frac{3}{2}}}, \\ -\frac{y(y^2-z^2)}{x(x^2+2y^2)^{3/2}}, -\frac{z(x^2+2y^2)}{x(x^2+2y^2)^{3/2}} \end{pmatrix}, \quad (50)$$

$$g = z\exp\left(\frac{x^2}{2y^2}\right) = V, \qquad h = \frac{x^2+y^2+z^2}{2x\sqrt{x^2+2y^2}} = W \quad (51)$$

The functions *f(x,y,z)* in Example 2 and *g* and *h* in Eq.51 also form an alternative spherical coordinate system. Click here to see this system in 3D.

Example 3:

Find the triple orthogonal coordinate surfaces to the surface family $f(x,y,x) = x^4 + y^4 + z^4 = U$.

Solution 3:

There is no function T that satisfies Equations 32-33. Although there is a function T that satisfies Equation 33, these values do not satisfy Equation 32. Therefore, there is no coordinate system orthogonal to the family in question or there are no triply orthogonal level surfaces (TOLS).

3 FAMILIES OF TRIPLY ORTHOGONAL PARAMETRIC SURFACES (TOPS)

If a function *T* cannot be found from Eqs.32-33 for the problem given in Equations 1-3, then all triple orthogonal surfaces cannot be expressed as level surfaces, and therefore a coordinate system cannot be considered. However, in such case families of triple perpendicular surfaces not of the form of Eq.2 can be found.

3.1 Finding Gradient Curves of Surfaces

For our known surface represented by the function *f(x,y,z)=U*, let $\vec{r}_1$ denote the curves perpendicular to the surface. $\vec{r}_1$curves

$$\dot{\vec{r}}_1 = (\dot{x}, \dot{y}, \dot{z}) = \vec{K} \quad (52)$$

can be found parametrically with a system of dynamic equations. A curve (say $\vec{r}_2$) on a given surface *f* will be perpendicular to the normal curve $\vec{r}_1$. To assign any surface curve on *f,* Eq.53 must be satisfied.

$$\dot{\vec{r}}_2 = (\dot{x}, \dot{y}, \dot{z}) = \vec{L}. \qquad (53)$$

The system of equations must be solved because it is known from Eq.21 that $\vec{r}_1 \cdot \vec{r}_2 = 0$. Similarly, to find the third family of perpendicular curves,

$$\dot{\vec{r}}_3 = \vec{M}. \qquad (54)$$

equation must be solved. Here, when finding the vectors *K, L* and *M*, we can assign any function T that does not need to satisfy Eq.37. If the systems of three equations in Eqs.52-54 are solved for the starting point (x_0, y_0, z_0) on the surface *f*,

$$\vec{r}(t) = \vec{r}_1(t, x_0, y_0, z_0), \qquad \vec{r}(t) = \vec{r}_2(t, x_0, y_0, z_0), \qquad \vec{r}(t) = \vec{r}_3(t, x_0, y_0, z_0) \qquad (55)$$

parametric vector functions are obtained (Fig.2). The gradient lines ($\vec{r}_2$ and $\vec{r}_3$) of the targeted surfaces are now ready. Note that $f(x_0, y_0, z_0) = U$ in this case.

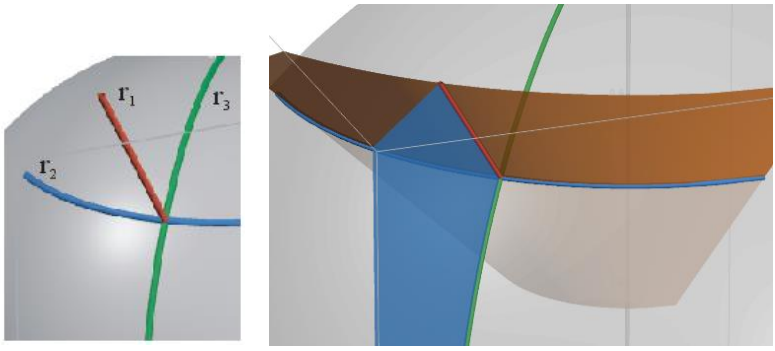

Fig.2: Perpendicular surface lines. Red perpendicular to the surface.

3.2 Finding Parametric Equations of Surfaces: Method of Parametric Surface Weaving

Let the surface formed by the union of $\vec{r}_1$ and $\vec{r}_2$ be denoted by $\vec{r}_{12}(u, v, x_0, y_0, z_0)$. Similarly, let the union of $\vec{r}_1$ and $\vec{r}_3$ be parametrically denoted by $\vec{r}_{13}(u, v, x_0, y_0, z_0)$. Suppose that (x_0, y_0, z_0) in $\vec{r}_1$ move on $\vec{r}_2$. In this case the *x, y, z* components of $\vec{r}_2$ will replace the initial conditions (x_0, y_0, z_0) of $\vec{r}_1$. To distinguish the pattern parameters *t*, let us substitute *u* for *t* in $\vec{r}_1$ and *v* for *t* in $\vec{r}_2$.

$$\vec{r}_1(u, x_0, y_0, z_0) = \begin{pmatrix} x_1(u, x_0, y_0, z_0) \\ y_1(u, x_0, y_0, z_0) \\ z_1(u, x_0, y_0, z_0) \end{pmatrix},$$

$$\vec{r}_2(v, x_0, y_0, z_0) = \begin{pmatrix} x_2(v, x_0, y_0, z_0) \\ y_2(v, x_0, y_0, z_0) \\ z_2(v, x_0, y_0, z_0) \end{pmatrix} \tag{56}$$

If x_0 in $\vec{r}_1$ is replaced by the function $x_2(v, x_0, y_0, z_0)$ which is the x component of $\vec{r}_2$, the surface $\vec{r}_{12}$ is obtained as in Eq.57.

$$\vec{r}_{12}(u, v) = \begin{pmatrix} x_1\big(u, x_2(v, x_0, y_0, z_0), y_2(v, x_0, y_0, z_0), z_2(v, x_0, y_0, z_0)\big) \\ y_1\big(u, x_2(v, x_0, y_0, z_0), y_2(v, x_0, y_0, z_0), z_2(v, x_0, y_0, z_0)\big) \\ z_1\big(u, x_2(v, x_0, y_0, z_0), y_2(v, x_0, y_0, z_0), z_2(v, x_0, y_0, z_0)\big) \end{pmatrix}. \tag{57}$$

The same algorithm can be applied for $\vec{r}_{13}$.

$$\vec{r}_{12}(u, v) = \begin{pmatrix} x_1\big(u, x_3(v, x_0, y_0, z_0), y_3(v, x_0, y_0, z_0), z_3(v, x_0, y_0, z_0)\big) \\ y_1\big(u, x_2(v, x_0, y_0, z_0), y_2(v, x_0, y_0, z_0), z_2(v, x_0, y_0, z_0)\big) \\ z_1\big(u, x_2(v, x_0, y_0, z_0), y_2(v, x_0, y_0, z_0), z_2(v, x_0, y_0, z_0)\big) \end{pmatrix}. \tag{58}$$

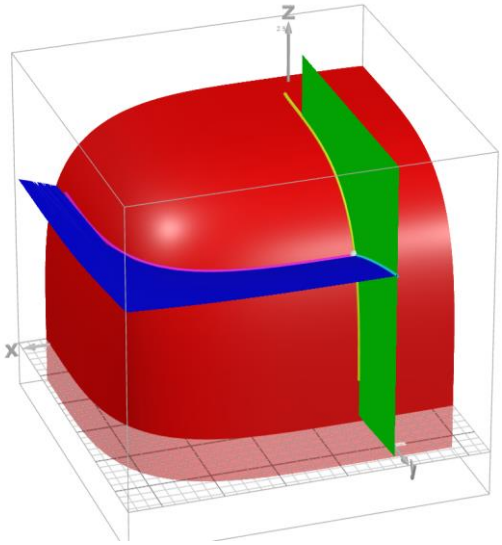

Fig.3: Orthogonal families of Example 4. Click here for the simulation.

Example 4: Find the triply orthogonal parametric surfaces (TOPS) to the surface family $f(x,y,x) = x^4 + y^4 + z^4 = U$.

These surfaces need not be in closed form. They can also be in parametric form.

Solution 4:

There is no need to find any value of T satisfying Equations 32-33 because the functions g and h do not have to be expressed as in Equation 2. Therefore, T=0 can be chosen for simplicity.

$$T = 0 \rightarrow \quad \vec{K} = (x^3, y^3, z^3), \qquad \vec{L} = (y^3, -x^3, 0), \qquad \vec{M} = (x^3z^3, y^3z^3, -x^6 - y^6). \tag{59}$$

Since the helicity density of the vector L is zero, the function g can be written in closed form ($g(x,y,z) = x^{-2} - y^{-2} = V$). However, the helicity density of the vector M is not zero, so it cannot be written as the gradient of a function of the form $h(x,y,z) = W$.

Let us consider the problem from a different perspective. Let's think of the vectors *K, L, M* not as the gradient of a scalar function, but as curves parallel to the vector fields. If we denote these three curves by $\vec{r}_1$, $\vec{r}_2$, $\vec{r}_3$, the tangent vectors of the curves must be proportional to *K, L, M*.

$$\dot{\vec{r}}_1(t) = \mu_1(x,y,z)\vec{K}, \qquad \dot{\vec{r}}_2(t) = \mu_2(x,y,z)\vec{L}, \qquad \dot{\vec{r}}_3(t) = \mu_3(x,y,z)\vec{M}. \tag{60}$$

In Equation 60, the functions $\mu_i(x,y,z)$ are functions that can be chosen to be useful in solving the problem. As can be seen in Eq.61, if $\mu_1 = 1, \mu_2 = x^{-3}y^{-3}, \mu_3 = z^{-3}$, Eq.62 is obtained.

$$\begin{aligned} \dot{x}(t) &= x^3 * \mu_1(x,y,z) & \dot{x}(t) &= y^3 * \mu_2(x,y,z) \\ \dot{y}(t) &= y^3 * \mu_1(x,y,z), & \dot{y}(t) &= -x^3 * \mu_2(x,y,z), \\ \dot{z}(t) &= z^3 * \mu_1(x,y,z) & \dot{z}(t) &= 0 \\ & & \dot{x}(t) &= x^3z^3 * \mu_3(x,y,z) \\ & & \dot{y}(t) &= y^3z^3 * \mu_3(x,y,z) \\ & & \dot{z}(t) &= -(x^6 + y^6) * \mu_3(x,y,z) \end{aligned} \tag{61}$$

$$\begin{aligned} \dot{x}(t) &= x^3 & \dot{x}(t) &= x^{-3} & \dot{x}(t) &= x^3 \\ \dot{y}(t) &= y^3, & \dot{y}(t) &= -y^{-3}, & \dot{y}(t) &= y^3 \\ \dot{z}(t) &= z^3 & \dot{z}(t) &= 0 & \dot{z}(t) &= -z^{-3}(x^6 + y^6) \end{aligned} \tag{62}$$

The solutions of the system of differential equations in Eq.62 are given in Eq.63.

$$\vec{r}_1 = \begin{pmatrix} (x_0^{-2} - 2t)^{-\frac{1}{2}} \\ (y_0^{-2} - 2t)^{-\frac{1}{2}} \\ (z_0^{-2} - 2t)^{-\frac{1}{2}} \end{pmatrix}, \qquad \vec{r}_2 = \begin{pmatrix} (x_0^4 + 4t)^{\frac{1}{4}} \\ (y_0^4 - 4t)^{\frac{1}{4}} \\ z_0 \end{pmatrix},$$
$$\vec{r}_3 = \begin{pmatrix} (x_0^{-2} - 2t)^{-1/2} \\ (y_0^{-2} - 2t)^{-1/2} \\ [z_0^4 + y_0^4 + x_0^4 - (x_0^{-2} - 2t)^{-2} - (y_0^{-2} - 2t)^{-2}]^{1/4} \end{pmatrix} \tag{63}$$

Here $\vec{r}_1$ represents the 3D curve perpendicular to the function f, our given reference surface. Similarly, $\vec{r}_2$ and $\vec{r}_3$ represent curves perpendicular to the functions g and h. Moreover, r2 and r3 will be on the f surface, r1 and r3 on the g surface, and $\vec{r}_1$ and $\vec{r}_2$ on the h surface (Fig.2). Since the curves $\vec{r}_2$ and $\vec{r}_3$ in Fig.2 are on the surface *f*, if the initial point (x_0, y_0, z_0) is moved over the surface *f*, the curves $\vec{r}_2$ and $\vec{r}_3$ will weave the surface *f*.

As described in Eq.56-57, after expressing $\vec{r}_1$ and $\vec{r}_2$ by the parameters u and v respectively, if x_0 in $\vec{r}_1$ is replaced by the *x* component of $\vec{r}_2$, the parametric surface $\vec{r}_{12}(u, v)$ is obtained as in Eq.64. That is, taking the vector $\vec{r}_1$ as reference, x_0, y_0, z_0 in $\vec{r}_1$ are replaced by $x_2(v)$, $y_2(v)$, $z_2(v)$ components *of* $\vec{r}_2$.

$$\vec{r}_1(u) = \begin{pmatrix} (x_0^{-2} - 2u)^{-\frac{1}{2}} \\ (y_0^{-2} - 2u)^{-\frac{1}{2}} \\ (z_0^{-2} - 2u)^{-\frac{1}{2}} \end{pmatrix}, \qquad \vec{r}_2(v) = \begin{pmatrix} (x_0^4 + 4v)^{\frac{1}{4}} \\ (y_0^4 - 4v)^{\frac{1}{4}} \\ z_0 \end{pmatrix} \rightarrow$$
$$\vec{r}_{12}(u, v) = \begin{pmatrix} \left((x_0^4 + 4v)^{1/4}\right)^{-2} - 2u\Big)^{-1/2} \\ \left((x_0^4 - 4v)^{1/4}\right)^{-2} - 2u\Big)^{-1/2} \\ ((z_0)^{-2} - 2u)^{-1/2} \end{pmatrix} \tag{64}$$

This method can also be reversed, i.e. taking vector $\vec{r}_2$ as a reference and replacing x_0, y_0, z_0 in $\vec{r}_2$ by the $x_1(v)$, $y_1(v)$, $z_1(v)$ components of r_1 (Eq.65).

$$\vec{r}_1(u) = \begin{pmatrix} (x_0^{-2} - 2u)^{-\frac{1}{2}} \\ (y_0^{-2} - 2u)^{-\frac{1}{2}} \\ (z_0^{-2} - 2u)^{-\frac{1}{2}} \end{pmatrix}, \qquad \vec{r}_2(v) = \begin{pmatrix} (x_0^4 + 4v)^{\frac{1}{4}} \\ (y_0^4 - 4v)^{\frac{1}{4}} \\ z_0 \end{pmatrix} \rightarrow$$

$$\vec{r}_{21}(u,v) = \begin{pmatrix} \left(\left((x_0^{-2} - 2u)^{-1/2}\right)^4 + 4v\right)^{1/4} \\ \left(\left((y_0^{-2} - 2u)^{-1/2}\right)^4 - 4v\right)^{1/4} \\ (z_0^{-2} - 2u)^{-1/2} \end{pmatrix} \tag{65}$$

Following a similar algorithm, the parametric surfaces $r_{13}(u,v)$, $r_{31}(u,v)$, $r_{23}(u,v)$, $r_{32}(u,v)$ are also found (Equations 66-69).

$$\vec{r}_{13}(u,v) = \begin{pmatrix} (x_0^{-2} - 2v - 2u)^{-1/2} \\ (y_0^{-2} - 2v - 2u)^{-1/2} \\ \left([z_0^4 + y_0^4 + x_0^4 - (x_0^{-2} - 2v)^{-2} - (y_0^{-2} - 2v)^{-2}]^{-1/2} - 2u\right)^{-1/2} \end{pmatrix} \tag{66}$$

$$\vec{r}_{31}(u,v) = \begin{pmatrix} (x_0^{-2} - 2u - 2v)^{-1/2} \\ (y_0^{-2} - 2u - 2v)^{-1/2} \\ \begin{bmatrix} (z_0^{-2} - 2u)^{-2} + (y_0^{-2} - 2u)^{-2} + (x_0^{-2} - 2u)^{-2} \\ -(x_0^{-2} - 2u - 2v)^{-2} - (y_0^{-2} - 2u - 2v)^{-2} \end{bmatrix}^{1/4} \end{pmatrix} \tag{67}$$

$$\vec{r}_{23}(u,v) = \begin{pmatrix} ((x_0^{-2} - 2v)^{-2} + 4u)^{1/4} \\ ((x_0^{-2} - 2v)^{-2} - 4u)^{1/4} \\ [z_0^4 + y_0^4 + x_0^4 - (x_0^{-2} - 2v)^{-2} - (y_0^{-2} - 2v)^{-2}]^{1/4} \end{pmatrix} \tag{68}$$

$$\vec{r}_{32}(u,v) = \begin{pmatrix} \left((x_0^4 + 4u)^{-1/2} - 2v\right)^{-1/2} \\ \left((y_0^4 - 4u)^{-1/2} - 2v\right)^{-1/2} \\ \begin{bmatrix} z_0^4 + y_0^4 + x_0^4 - \left((x_0^4 + 4u)^{-\frac{1}{2}} - 2v\right)^{-2} \\ -\left((y_0^4 - 4u)^{-1/2} - 2v\right)^{-2} \end{bmatrix}^{1/4} \end{pmatrix} \tag{69}$$

Click here for the graphical software showing the solution of this example. Cartesian forms of the surfaces may be seen in Table 3.

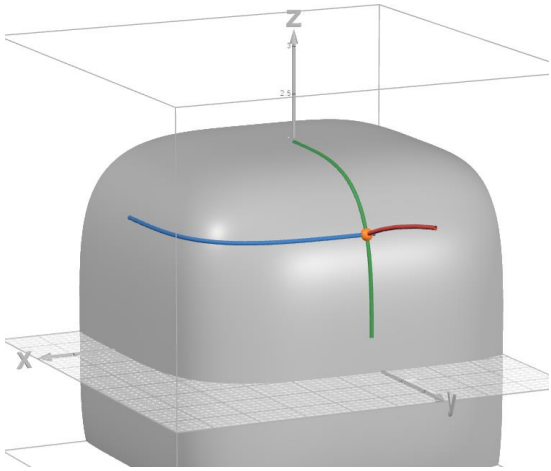

Fig.4: $\vec{r}_1$ is shown in red, $\vec{r}_2$ in blue, $\vec{r}_3$ in green. Initial point (x_0,y_0,z_0) is shown in orange point.

4 RESULTS AND DISCUSSIONS

4.1 Explanation of the MATLAB Script in Appendix A

The MATLAB command directory in Appendix A was used to find the results. When the function f is substituted and the script is run, the following values will appear in the results: Darboux_Cayley_det, ABC, Zero_solution, T_solved, DotKLM, Helicity_Densities, L_final, M_final (Table 1).

Table 1: Names and Explanations of the outputs obtained from Appendix A.

Parameter name	**Explanation**
Darboux_Cayley_det	If this value is zero, the Darboux-Cayley condition is satisfied.
ABC	It gives the 6 coefficients in Eq.33.
Zero_solution	If this 2x1 vector is zero, a function T satisfying Eq.32 is found.
T_solved	It gives the functions T which are the solution of Eq.33.
DotKLM	If this 3x1 vector is zero, then the vectors K,L,M are perpendicular. It can be used for control purposes.
Helicity_Densities	If this vector is zero, then the helicity densities of L and M are zero. For control purposes.
L_final	The resulting simplest L vector.
M_final	The resulting simplest M vector.

If the "*Zero_solution*" parameter is zero, the "*T_solved"* parameter is automatically substituted in the script and the program gives the final correct L and M vectors. Once vectors *L* and *M* are obtained, *g(x,y,z)* and *h(x,y,z)* can be found manually as described in Section 2.5. If the "*Zero_solution*" parameter is not zero, then there is no suitable *T(x,y,z)* function and the surface families *f(x,y,z)* entered into the program cannot form an orthogonal coordinate system.

4.2 Some Triply Orthogonal Surface Families

Finding families of triple orthogonal surfaces without any restrictions requires looking for functions g and h which are gradient vectors parallel to the vectors L and M given by Eq.21-22 for an arbitrary function T. However, if these families of surfaces are expected to be in the form of level surfaces as in Eq.1-3, the function T should not be chosen randomly, but in a way that satisfies Eq.33. In this case a triple orthogonal coordinate system can be obtained. Finding a triple orthogonal coordinate system is described in section 2 and finding any family of triple orthogonal surfaces is described in Chapter 3. Some triple orthogonal coordinate systems (TOLS) found by these methods are listed in Table 2 and general families of triple orthogonal surfaces (TOPS) are listed in Table 3.

Example 5:

Find the triple orthogonal coordinate surfaces to the surface family $f(x,y,z) = xyz = U$

Solution 5:

When the MATLAB command in Appendix A is run, some of the results obtained are shown in Table 3. The values of "*Darboux_Cayley_det*" (Kasner, 1911) and "*Zero_solution*" are zero, indicating that a triple orthogonal coordinate system can be found for this surface family. "*T_solved*" came out as one set. This means that only one triple orthogonal coordinate system can be written, which can only be found by continuing by substituting the "T_solved" value given in Table 4.

Table 4: Part of the results obtained from the MATLAB command for the function *f=xyz*.

Darboux_Cayley_det	ABC	Zero_solution	T_solved
0	[0, -y*(x^2 - z^2)*(x^2*y^2 + x^2*z^2 + y^2*z^2), 0]	0	(z*(x^4 - x^2*y^2 - x^2*z^2 + y^4 - y^2*z^2 + z^4)^(1/2) - x^2*z + z^3)/(x*y^2 - x*z^2)
	[2*x^3*y*z*(y^2 - z^2), -y*(x^2 - z^2)*(x^2*y^2 - 3*x^2*z^2 + y^2*z^2), 2*x*y*z^3*(x^2 - y^2)]	0	-(z*(x^4 - x^2*y^2 - x^2*z^2 + y^4 - y^2*z^2 + z^4)^(1/2) + x^2*z - z^3)/(x*y^2 - x*z^2)

If the triple orthogonal coordinate system must be found, the MATLAB code continues for the given "*T_solved*", resulting in the values in Table 4. If the scalar functions *g* and *h* whose gradients are parallel to the vectors *L* and *M* here, Example 5 will be solved, and the orthogonal coordinate system will be found. However, this solution is too long and complicated and is not the subject of this paper.

Table 5: Vectors *L* and *M* required for the function $f(x, y, z) = xyz$ to be a triple orthogonal coordinate system.

L_final	x*(y^2 - z^2) -y*((x^4 - x^2*y^2 - x^2*z^2 + y^4 - y^2*z^2 + z^4)^(1/2) - x^2 + y^2) z*((x^4 - x^2*y^2 - x^2*z^2 + y^4 - y^2*z^2 + z^4)^(1/2) - x^2 + z^2)
M_final	x*(y^2*(x^4 - x^2*y^2 - x^2*z^2 + y^4 - y^2*z^2 + z^4)^(1/2) - x^2*z^2 - x^2*y^2 + z^2*(x^4 - x^2*y^2 - x^2*z^2 + y^4 - y^2*z^2 + z^4)^(1/2) + y^4 + z^4) -y*(z^2*(x^4 - x^2*y^2 - x^2*z^2 + y^4 - y^2*z^2 + z^4)^(1/2) - x^2*y^2 + z^4) -z*(y^2*(x^4 - x^2*y^2 - x^2*z^2 + y^4 - y^2*z^2 + z^4)^(1/2) - x^2*z^2 + y^4)

Table 2: Examples of functions *f, g, h* that can be written as orthogonal coordinates (TOLS).

	f	T	g	h	Link	
1	$x^2+y^2+z^2=U$	0	$\frac{y}{x}=V$	$\frac{x^2+y^2}{z^2}=W$	Spherical 1	
2	$x^2+y^2+z^2=U$	p	$\frac{y}{x+pz}=V$	$\frac{x^2+y^2+z^2}{(z-px)^2}=W$	Spherical 2	
3	$x^2+y^2+z^2=U$	$\frac{y^2}{xz}$	$z\exp\left(\frac{x^2}{2y^2}\right)=V$	$\frac{x^2+y^2+z^2}{2x\sqrt{x^2+2y^2}}=W$	Spherical 3	
4	$\frac{x^p y^q}{z^{p+q}}=U$	$\frac{z}{x}$	$x^2+y^2+z^2=V$	$\frac{(p+q)y^2+qz^2}{(p+q)x^2+pz^2}=W$	Spherical 4	
4.a	$\frac{xy}{z^2}=U$	$\frac{z}{x}$	$x^2+y^2+z^2=V$	$\frac{2y^2+z^2}{2x^2+z^2}=W$	Spherical 5	
5	$x^2+y^2+pz^2=U$	0	$\frac{y}{x}=V$	$z^2(x^2+y^2)^{-p}=W$	Spheroidal	
5.a	$x^2+y^2-z^2=U$	0	$\frac{y}{x}=V$	$z^2(x^2+y^2)=W$	Hyperboloid	
5.b	$x^2+y^2+2z^2=U$	$-\frac{x}{y}$	$\frac{y}{x}=V$	$\frac{x^2+y^2}{z}=W$		
5.c	$x^2+y^2+\frac{1}{2}z^2=U$	$-\frac{x}{y}$	$\frac{y}{x}=V$	$\frac{x^2+y^2}{z^4}=W$		
6	$x^2+y^2+pz^q=U$	0	$\frac{y}{x}=V$	$\frac{\exp(4z^{2-q})}{(x^2+y^2)^{pq(2-q)}}=W$	Superellipsoidal1	$q\neq 2$
6.a	$\frac{y}{x}=U$	$\frac{1}{x}$	$2z+x^2+y^2=V$	$\frac{e^{2z}}{x^2+y^2}=W$	Paraboloidal	
6.b	$x^2+y^2-z=U$	$-\frac{x}{y}$	$\frac{y}{x}=V$	$(x^2+y^2)e^{4z}=W$		
7	$(x^2+y^2)^p+az^q=U$	0	$\frac{y}{x}=V$	$4p(1-p)z^{2-q}-aq(2-q)(x^2+y^2)^{1-p}$	Superellipsoidal2	$p\neq 1$ $q\neq 2$

						(p,q) $\neq (0,0)$
7.a	$z^3-(x^2+y^2)^2=U$	$-\frac{x}{y}$	$\frac{y}{x}=V$	$\frac{3}{x^2+y^2}+\frac{8}{z}=W$	Simulation	
8	$\left(\sqrt{x^2+y^2}-R\right)^2+z^2=a^2$	0	$\frac{y}{x}=V$	$\frac{\sqrt{x^2+y^2}-R}{z}=W$	Toroidal 1	
9	$\sqrt{x^2+y^2}+s\sqrt{a^2-z^2}=R$	0	$\frac{y}{x}=V$	$s\sqrt{x^2+y^2}+\sqrt{a^2-z^2}-a*\operatorname{arctanh}\frac{\sqrt{a^2-z^2}}{a}=W$	Toroidal 2	$s=\pm 1$
10	$x^2+y+z=U$	∞	$y-z=V$	$\frac{1}{x}\exp(y+z)=W$	Simulation	
11	$z^2-2xy=U$	1	$\frac{y-x}{z}=V$	$2z^2(x+y)^2+(y^2-x^2)^2=W$	Simulation	
12	$\frac{x^2+y^2+z^2}{x}=U$	∞	$\frac{z}{y}=V$	$\frac{x^2}{\sqrt{y^2+z^2}}+\sqrt{y^2+z^2}=W$		
13	$\frac{x^2+y^2+z^2}{z}=U$	$-\frac{x}{y}$	$\frac{y}{x}=V$	$\frac{z^2}{\sqrt{x^2+y^2}}+\sqrt{x^2+y^2}=W$		
14*	$xyz=U$				T=T_s^*	

14* If we take $T_s=\frac{z(x^4-x^2y^2-x^2z^2+y^4-y^2z^2+z^4)^{\frac{1}{2}}-x^2z+z^3}{xy^2-xz^2}$, the surface families of $f=xyz=U$ belong to an orthogonal coordinate system. However, since it is very difficult to find these orthogonal surface families, they are not discussed here. For the verification of orthogonality of functions *f, g, h*, use Appendix C.

Table 3: Examples of triple orthogonal parametric surfaces (TOPS) *f, g, h* that can be written in parametric form, or simply, that cannot be any coordinates.

	f	T	g	h	Link
1	$\vec{r}_{32} = \begin{bmatrix} ((x_0^{-2} - 2v)^{-2} + 4u)^{1/4} \\ ((y_0^{-2} - 2v)^{-2} - 4u)^{1/4} \\ \left(x_0^4 + y_0^4 + z_0^4 - (x_0^{-2} - 2v)^{-2} - \right)^{1/4} \\ (y_0^{-2} - 2v)^{-2} \end{bmatrix}$ $x^4 + y^4 + z^4 = x_0^4 + y_0^4 + z_0^4$	0	$\vec{r}_{21} = \begin{bmatrix} ((x_0^{-2} - 2u)^{-2} + 4v)^{1/4} \\ ((y_0^{-2} - 2u)^{-2} - 4u)^{1/4} \\ (z_0^{-2} - 2u)^{-1/2} \end{bmatrix}$ $\frac{y^2 - x^2}{x^2 y^2} = \frac{y_0^2 - x_0^2}{x_0^2 y_0^2}$	$\vec{r}_{13} = \begin{bmatrix} (x_0^{-2} - 2u - 2v)^{-1/2} \\ (y_0^{-2} - 2u - 2v)^{-1/2} \\ \left(\left(x_0^4 + y_0^4 + z_0^4 - (x_0^{-2} - 2v)^{-2}\right)^{-\frac{1}{2}} - 2u\right)^{-1/2} \\ -(y_0^{-2} - 2v)^{-2} \end{bmatrix}$ $x^4 + y^4 = (z^{-2} - z_0^{-2} + x_0^{-2})^{-2} + (z^{-2} - z_0^{-2} + y_0^{-2})^{-2}$	Sim.
2	$\vec{r}_{23} = \begin{bmatrix} \frac{x_0 y_0 z_0}{\sqrt{z_0^2 + 2v}\sqrt{y_0^2 + 2v}} \\ \sqrt{y_0^2 + 2v}\exp u \\ \sqrt{z_0^2 + 2v}\exp(-u) \end{bmatrix}$ $xyz = x_0 y_0 z_0$	∞	$\vec{r}_{12} = \begin{bmatrix} \sqrt{x_0^2 + 2v} \\ \sqrt{y_0^2 + 2v}\exp(u) \\ \sqrt{z_0^2 + 2v}\exp(-u) \end{bmatrix}$ $y^2 - z^2 = y_0^2 - z_0^2$	$\vec{r}_{23} = \begin{bmatrix} \frac{x_0 y_0 z_0}{\sqrt{z_0^2 + 2v}\sqrt{y_0^2 + 2v}} \\ \sqrt{y_0^2 + 2v}\exp u \\ \sqrt{z_0^2 + 2v}\exp(-u) \end{bmatrix}$ $(x^2 + y_0^2 - x_0^2)(x^2 + z_0^2 - x_0^2) = y^2 z^2$	Sim.

3	$\vec{r}_{23} = \begin{bmatrix} \sqrt{x_0^2 + 4v}\exp(-u) \\ \sqrt{y_0^2 + 2v}\exp u \\ \sqrt{z_0^2 - x_0y_0 + \sqrt{x_0^2 + 4v}\sqrt{y_0^2 + 4v}} \end{bmatrix}$ $xy - z^2 = x_0y_0 - z_0^2$	0	$\vec{r}_{13} = \begin{bmatrix} \sqrt{x_0^2 + 4v + 2u} \\ \sqrt{y_0^2 + 4v + 2u} \\ \frac{\sqrt{z_0^2 - x_0y_0 + \sqrt{x_0^2 + 4v}\sqrt{y_0^2 + 4v}}\left(\sqrt{x_0^2 + 4v} + \sqrt{y_0^2 + 4v}\right)^2}{x_0^2 + y_0^2 + 8v + 4u + 2\sqrt{x_0^2 + 4v + 2u}\sqrt{y_0^2 + 4v + 2u}} \end{bmatrix}$ $x^2 - y^2 = x_0^2 - y_0^2$	$\vec{r}_{21} = \begin{bmatrix} \sqrt{x_0^2 + 2v}\exp(-u) \\ \sqrt{y_0^2 + 2v}\exp(u) \\ \frac{z_0(x_0 + y_0)^2}{x_0^2 + y_0^2 + 4v + 2\sqrt{x_0^2 + 2v}\sqrt{y_0^2 + 2v}} \end{bmatrix}$ $(x_0 - y_0)^2z^2 + 4z_0xyz = z_0^2(x_0 + y_0)^2$	Sim.
4	$\vec{r}_{23} = \begin{bmatrix} \sqrt{x_0^2\exp(6v) + 4u} \\ \sqrt{y_0^2\exp(12v) - 2u} \\ \frac{1}{\sqrt{3}}\sqrt{x_0^2 + 2y_0^2 + 3z_0^2 - x_0^2\exp(6v) - 2y_0^2\exp 12v} \end{bmatrix}$ $x^2 + 2y^2 + 3z^2 = U$	0	$\vec{r}_{13} = \begin{bmatrix} x_0\exp(3v)\exp(u) \\ y_0\exp(6v)\exp(2u) \\ \frac{\exp(3u)}{\sqrt{3}} * \sqrt{x_0^2 + 2y_0^2 + 3z_0^2 - x_0^2\exp(6v) - 2y_0^2\exp 12v} \end{bmatrix}$ $\frac{y}{x^2} = \frac{y_0}{x_0^2}$	$\vec{r}_{21} = \begin{bmatrix} \sqrt{x_0^2\exp(2v) + 4u} \\ \sqrt{y_0^2\exp(4v) - 2u} \\ z_0\exp(3v) \end{bmatrix}$ $x^2 + 2y^2 = x_0^2(z/z_0)^{2/3} + 2y_0^2(z/z_0)^{4/3}$	Sim.

* To verify the triple orthogonality of surfaces written in parametric form, readers can use the MATLAB script given in Appendix D

Example 6:

Find any set of triple orthogonal surface family to the surface family of $f(x,y,z) = xyz = U$

Solution 6:

If the "Td" value in the MATLAB file is written as zero, a set of perpendicular surface families without a coordinate system can be obtained. According to the ABC values in Table 3, A1=C1=0. Since C1=0, the choice of T=0 at least satisfies the principal equation of Eq.32, i.e. only the function g can be written as a closed form coordinate family. In this case, the L and M vectors are as shown in Table 6.

Table 6: Vectors *L* and *M* when *Td=0* for the function $f(x,y,z) = xyz$.

L_final	x -y 0
M_final	x*y^2 x^2*y -z*(x^2 + y^2)

The helicity density of vector *L* in Table 6 is zero, while that of *M* is non-zero. This can be seen from the result of the "*Helicity_Densities*" parameter in MATLAB results. This means that a gradient parallel to vector *L* can be found, but not for *M*. It is best to find this solution with parametric methods.

$$\vec{r}_1(t) = \mu_1(x,y,z)\begin{pmatrix} yz \\ xz \\ xy \end{pmatrix}, \qquad \vec{r}_2(t) = \mu_2(x,y,z)\begin{pmatrix} x \\ -y \\ 0 \end{pmatrix},$$
$$\vec{r}_3(t) = \mu_3(x,y,z)\begin{pmatrix} xy^2 \\ x^2y \\ -z(x^2+y^2) \end{pmatrix}. \tag{70}$$

In Equation 70, the functions $\mu_i(x,y,z)$ are functions that can be chosen to be useful in solving the problem. If $\mu_1 = 1/xyz, \mu_2 = 1, \mu_3 = 1/x^2y^2$, Eq.71 is obtained.

$$\begin{array}{lll} & \dot{x}(t) = 1/x & \dot{x}(t) = x \\ for\ \vec{r}_1, & \dot{y}(t) = 1/y, & for\ \vec{r}_2, \quad \dot{y}(t) = -y, \\ & \dot{z}(t) = 1/z & \dot{z}(t) = 0 \\ & & \dot{x}(t) = 1/x \\ & for\ \vec{r}_3, & \dot{y}(t) = 1/y \\ & & \dot{z}(t) = -z(1/x^2 + 1/y^2) \end{array} \tag{71}$$

The solutions of Eq.71 are given in Eq.72.

$$\vec{r}_1(t) = \begin{pmatrix} \sqrt{x_0^2 + 2t} \\ \sqrt{y_0^2 + 2t} \\ \sqrt{z_0^2 + 2t} \end{pmatrix}, \qquad \vec{r}_2(t) = \begin{pmatrix} x_0 e^t \\ y_0 e^{-t} \\ z_0 \end{pmatrix}, \vec{r}_3(t) = \begin{pmatrix} \sqrt{x_0^2 + 2t} \\ \sqrt{y_0^2 + 2t} \\ \dfrac{x_0 y_0 z_0}{\sqrt{x_0^2 + 2t}\sqrt{y_0^2 + 2t}} \end{pmatrix}. \tag{72}$$

The curves seen in Eq.72 are orthogonal. While the curve $\vec{r}_1$ is perpendicular (normal) to the surface families $xyz = U$, $\vec{r}_2$ and $\vec{r}_3$ are on these surface families and perpendicular to each other. Moving on the curves $\vec{r}_2$, the combination of the normal curves $\vec{r}_1$ will form the surface given by $\vec{r}_{21}$. The parametric finding of this surface is given in Eq.73.

$$\vec{r}_2(u) = \begin{pmatrix} x_0 e^u \\ y_0 e^{-u} \\ z_0 \end{pmatrix} \rightarrow \vec{r}_1(v) = \begin{pmatrix} \sqrt{x_0^2 + 2v} \\ \sqrt{y_0^2 + 2v} \\ \sqrt{z_0^2 + 2v} \end{pmatrix} \rightarrow \vec{r}_{21}(u, v) = \begin{pmatrix} \sqrt{x_0^2 + 2v}e^u \\ \sqrt{y_0^2 + 2v}e^{-u} \\ \sqrt{z_0^2 + 2v} \end{pmatrix}. \tag{73}$$

Similarly, moving on the curves $\vec{r}_1$, the combination of the curves $\vec{r}_1$ will form the surface given by $\vec{r}_{13}$. The parametric finding of this surface is given in Eq.74.

$$\vec{r}_1(u) = \begin{pmatrix} \sqrt{x_0^2 + 2u} \\ \sqrt{y_0^2 + 2u} \\ \sqrt{z_0^2 + 2u} \end{pmatrix} \rightarrow \vec{r}_3(v) = \begin{pmatrix} \sqrt{x_0^2 + 2v} \\ \sqrt{y_0^2 + 2v} \\ \dfrac{x_0 y_0 z_0}{\sqrt{x_0^2 + 2v}\sqrt{y_0^2 + 2v}} \end{pmatrix}$$

$$\rightarrow \vec{r}_{13}(u, v) = \begin{pmatrix} \sqrt{x_0^2 + 2v + 2u} \\ \sqrt{y_0^2 + 2v + 2u} \\ \sqrt{\dfrac{x_0^2 y_0^2 z_0^2}{(x_0^2 + 2v)(y_0^2 + 2v)} + 2u} \end{pmatrix}. \quad (74)$$

Consequently, Eq.73-74 and the given parametric surface families $\vec{r}_{21}$ and $\vec{r}_{13}$ are orthogonal to the surface families given in Example 5. These surfaces given in parametric form can also be written in Cartesian form. In the product of the *x* and *y* components of the parametric surface at $\vec{r}_{21}$ the parameter u vanishes and the *xy* value is expressed depending only on *v*. Hence, if the *z* component and the parameter *v* are eliminated,

$$(z^2 + x_0^2 - z_0^2)(z^2 + y_0^2 - z_0^2) = x^2 y^2$$

is obtained. For the surface $\vec{r}_{13}$, when the squared difference of x and y is taken, *u* and *v* disappear. This way,

$$y^2 - x^2 = y_0^2 - x_0^2 \quad (76)$$

is found. Click here for a simulation showing the result of this example.

5 CONCLUSIONS

This study presents a comprehensive framework for determining and constructing three-fold orthogonal systems, offering significant contributions to both the theoretical and practical aspects of differential geometry. The main findings and conclusions of this research are summarized as follows:

- For a given family of level surfaces, it has been proven that, under certain conditions, two additional surface families orthogonal to each other and to the given family can be identified. Explicit methods have been proposed for determining these conditions and exploring the associated coordinate systems.

- By utilizing gradient-based approaches and helicity density conditions, this study establishes a systematic framework to verify whether specific surface families can form triple orthogonal coordinate systems. The derived equations, particularly the existence of the T-function, play a central role in addressing this problem. Additionally, a MATLAB-based computational tool was developed to automate the verification and exploration process. This tool not only simplifies algebraic complexity but also demonstrates how theoretical frameworks can be effectively applied in practice.
- In cases where three-fold orthogonal systems cannot be represented in closed forms, this research introduces methods for constructing parametric surface families while preserving orthogonality. This approach enables the discovery of diverse sets of orthogonal surface families, extending beyond coordinate systems. Such flexibility is particularly valuable for researchers engaged in visual or artistic studies alongside analytical investigations.
- The methodology has been successfully demonstrated through numerous examples, encompassing classical coordinate systems (e.g., Cartesian, spherical, and ellipsoidal) and customized configurations tailored to specific geometries. The integration of computational tools further facilitates real-time applications in fields such as geodesy, fluid dynamics, and electromagnetic theory. With results that are mathematically validated and graphically confirmed, all proposed methods and examples can be confidently utilized.

APPENDIX A

```
close all; clear all; clc;
syms x y z T A B u v x0 y0 z0 t p q
X=[x;y;z];
f=x^2+y^2+z^3; % Type the reference surface

fx=diff(f,x); fy=diff(f,y); fz=diff(f,z); fxx=diff(f,x,2); fyy=diff(f,y,2); fzz=diff(f,z,2); fxy=diff(f,x,y);
fxz=diff(f,x,z); fyz=diff(f,y,z);
H=1/sqrt(fx^2+fy^2+fz^2); Hxx=diff(H,x,2); Hyy=diff(H,y,2); Hzz=diff(H,z,2); Hxy=diff(H,x,y);
Hxz=diff(H,x,z); Hyz=diff(H,y,z);
Matrix=[Hxx Hyy Hzz Hyz Hxz Hxy;fxx fyy fzz fyz fxz fxy;1 1 1 0 0 0;2*fx 0 0 0 fz fy;0 2*fy 0 fz 0 fx;0
0 2*fz fy fx 0];
```

```
Darboux_Cayley_det =simplify(det(Matrix),'IgnoreAnalyticConstraints',true) % Darboux-Cayley
Determinat

[nx, dx] = numden(fx); [ny, dy] = numden(fy); [nz, dz] = numden(fz);
K1=simplify(expand(fx*lcm(lcm(dx,dy),dz)),'IgnoreAnalyticConstraints',true);
K2=simplify(expand(fy*lcm(lcm(dx,dy),dz)),'IgnoreAnalyticConstraints',true);
K3=simplify(expand(fz*lcm(lcm(dx,dy),dz)),'IgnoreAnalyticConstraints',true);
lm=[K2;-K1;0]; l=[0;-K3;K2]; mu=[K1*K3;K2*K3;-K1^2-K2^2]; m=[K2^2+K3^2;-K1*K2;-K1*K3];
Cl=curl(l,X); Clm=curl(lm,X); Cm=curl(m,X); Cmu=curl(mu,X);

A1=simplify((K1^2+K2^2+K3^2)*(l(1)*Cl(1)+l(2)*Cl(2)+l(3)*Cl(3)),'IgnoreAnalyticConstraints',true);
A2=simplify((m(1)*Cm(1)+m(2)*Cm(2)+m(3)*Cm(3)),'IgnoreAnalyticConstraints',true);
C1=simplify((K1^2+K2^2+K3^2)*(lm(1)*Clm(1)+lm(2)*Clm(2)+lm(3)*Clm(3)),'IgnoreAnalyticConstrai
nts',true);
C2=simplify((mu(1)*Cmu(1)+mu(2)*Cmu(2)+mu(3)*Cmu(3)),'IgnoreAnalyticConstraints',true);
B1=simplify((K1^2+K2^2+K3^2)*(l(1)*Clm(1)+l(2)*Clm(2)+l(3)*Clm(3) +
lm(1)*Cl(1)+lm(2)*Cl(2)+lm(3)*Cl(3)),'IgnoreAnalyticConstraints',true);
B2=simplify(m(1)*Cmu(1)+m(2)*Cmu(2)+m(3)*Cmu(3) +
mu(1)*Cm(1)+mu(2)*Cm(2)+mu(3)*Cm(3),'IgnoreAnalyticConstraints',true);
ABC=[A1 B1 C1;A2 B2 C2] % the six coeeficiets for T(x,y,z)

E=(A1-A2)*T^2+(B1-B2)*T+C1-C2;
Ts = solve(E,T); % candicate for T(x,y,z)

% If Zero1 and Zero2 give 0, Ts satisfies the condition
Zero1=simplify(K2*(K1^2+K2^2+K3^2)*(K1*diff(Ts(1),x)+K2*diff(Ts(1),y)+K3*diff(Ts(1),z)) +
A1*Ts(1)^2 + B1*Ts(1) + C1,'IgnoreAnalyticConstraints',true);
Zero2=simplify(K2*(K1^2+K2^2+K3^2)*(K1*diff(Ts(2),x)+K2*diff(Ts(2),y)+K3*diff(Ts(2),z)) +
A1*Ts(2)^2 + B1*Ts(2) + C1,'IgnoreAnalyticConstraints',true);
Zero_solution=[Zero1;Zero2]

T_solved=[Ts(1);Ts(2)]

Td=simplify(expand(Ts(1)),'IgnoreAnalyticConstraints',true);

L1=simplify(expand(K2),'IgnoreAnalyticConstraints',true);
L2=simplify(expand(-K1-K3*Td),'IgnoreAnalyticConstraints',true);
L3=simplify(expand(K2*Td),'IgnoreAnalyticConstraints',true);
M1=simplify(expand(K1*K3+(K2^2+K3^2)*Td),'IgnoreAnalyticConstraints',true);
M2=simplify(expand(K2*K3-K1*K2*Td),'IgnoreAnalyticConstraints',true);
M3=simplify(expand(-K1^2-K2^2-K1*K3*Td),'IgnoreAnalyticConstraints',true);

K=[K1;K2;K3]; L=[L1;L2;L3]; M=[M1;M2;M3];
DotKL=simplify(K1*L1+K2*L2+K3*L3); DotKM=simplify(K1*M1+K2*M2+K3*M3);
DotML=simplify(M1*L1+M2*L2+M3*L3);
DotKLM=[DotKL DotKM DotML]  % check that it is zero
```

```
HD_L=simplify(L(1)*(diff(L(3),y)-diff(L(2),z)) + L(2)*(diff(L(1),z)-diff(L(3),x)) + L(3)*(diff(L(2),x)-
diff(L(1),y)),'IgnoreAnalyticConstraints',true);
HD_M=simplify(M(1)*(diff(M(3),y)-diff(M(2),z)) + M(2)*(diff(M(1),z)-diff(M(3),x)) +
M(3)*(diff(M(2),x)-diff(M(1),y)),'IgnoreAnalyticConstraints',true);
Helicity_Densities=[HD_L HD_M] % check the helicity densities


[~, d1] = numden(K(1)); [~, d2] = numden(K(2)); [~, d3] = numden(K(3)); common_denominator =
lcm(lcm(d1, d2), d3); K_poly = K * common_denominator; common_factor = K_poly(1);
for i = 2:length(K_poly)
    common_factor = gcd(common_factor, K_poly(i));
end
K_final = simplify(K_poly / common_factor,'IgnoreAnalyticConstraints',true);

[~, d1] = numden(L(1)); [~, d2] = numden(L(2)); [~, d3] = numden(L(3)); common_denominator =
lcm(lcm(d1, d2), d3); L_poly = L * common_denominator; common_factor = L_poly(1);
for i = 2:length(L_poly)
    common_factor = gcd(common_factor, L_poly(i));
end
L_final = simplify(L_poly / common_factor,'IgnoreAnalyticConstraints',true)

[~, d1] = numden(M(1)); [~, d2] = numden(M(2)); [~, d3] = numden(M(3)); common_denominator =
lcm(lcm(d1, d2), d3); M_poly = M * common_denominator; common_factor = M_poly(1);
for i = 2:length(M_poly)
    common_factor = gcd(common_factor, M_poly(i));
end
M_final = simplify(M_poly / common_factor,'IgnoreAnalyticConstraints',true)

%KLM=[K_final L_final M_final] % final and simplified K, L, M vectors
```

APPENDIX B

Surface of Revolution

All rotational surfaces in *xyz* space can be written with rotation and translation transformations such that the axis of rotation is the z-axis. In this case our given reference surface *f(x,y,z)* is written as in Eq.A1.

$$f(r,z) = U, \qquad r = \sqrt{x^2 + y^2} \tag{A1}$$

In this case, $\vec{\lambda}$ and $\vec{\mu}$ given in Eq.23-24 are as shown in Eq.A2-A3.

$$\vec{\lambda} = \left(f_y, -f_x, 0\right) = f_r \sin\theta\, \hat{x} - f_r \cos\theta\, \hat{y} \tag{A2}$$

$$\vec{\mu} = \left(f_x f_z, f_y f_z, -f_x^2 - f_y^2\right) = f_r f_z \cos\theta\, \hat{x} + f_r f_z \sin\theta\, \hat{y} - f_r^2 \hat{z}, \tag{A3}$$

The expression of these vectors in cylindrical coordinates is described in Eq.A4-6.

$$\hat{r} = \cos\theta\,\hat{x} + \sin\theta\,\hat{y}, \qquad \hat{\theta} = -\sin\theta\,\hat{x} + \cos\theta\,\hat{y} \quad \text{(A4)}$$

$$\vec{\lambda} = (\vec{\lambda}\cdot\hat{r})\hat{r} + (\vec{\lambda}\cdot\hat{\theta})\hat{\theta} + (\vec{\lambda}\cdot\hat{z})\hat{z} = f_r\hat{\theta} \quad \text{(A5)}$$

$$\vec{\mu} = (\vec{\mu}\cdot\hat{r})\hat{r} + (\vec{\mu}\cdot\hat{\theta})\hat{\theta} + (\vec{\mu}\cdot\hat{z})\hat{z} = f_r f_z\hat{r} - f_r^2\hat{z} \quad \text{(A6)}$$

When the functions C_1 and C_2 defined in Eq.30-31 are written for the vectors in Eq.A5-6, they always give zero (Eq.A6-7). The curl of the vectors was found by the curl formula in cylindrical coordinates.

$$\vec{\nabla}\times\vec{\lambda} = (-f_{rz})\hat{r} + (f_r + rf_{rr})\hat{z} \quad \rightarrow \quad C_1 = \vec{\lambda}\cdot\nabla\times\vec{\lambda} = 0 \quad \text{(A7)}$$

$$\vec{\nabla}\times\vec{\mu} = ((f_r f_z)_z + (f_r^2)_r)\hat{\theta} \quad \rightarrow \quad C_2 = \vec{\mu}\cdot\nabla\times\vec{\mu} = 0 \quad \text{(A8)}$$

Consequently, given a family of rotational surfaces, C1 and C2 will definitely be zero. The orthogonal coordinate system condition of Eq.32-33 will be satisfied for T=0. So, in the case that *f(x,y,z)* is a rotational surface, there can only be one orthogonal coordinate system for T=0.

The expression for the gradient in cylindrical coordinates is given in Eq.9. Also, for T=0 the vectors L and M, i.e. the vectors parallel to the gradient of the families of faces g and h, are given in Eq.A11-12.

$$\vec{\nabla}g = g_r\hat{r} + \frac{1}{r}g_\theta\hat{\theta} + g_z\hat{z}, \qquad \vec{\nabla}h = h_r\hat{r} + \frac{1}{r}h_\theta\hat{\theta} + h_z\hat{z} \quad \text{(A9)}$$

$$\vec{L} = \vec{\lambda} = (K_2, -K_1, 0) = f_r\hat{\theta} \quad \text{(A11)}$$

$$\vec{M} = \vec{\mu} = \left(K_1K_3, K_2K_3, -(K_1^2 + K_2^2)\right) = f_r f_z\hat{r} - f_r^2\hat{z} \quad \text{(A12)}$$

If the components of the L and M vectors are multiplied by the necessary functions to satisfy $\vec{\nabla}g \parallel \vec{L}$ and $\vec{\nabla}h \parallel \vec{M}$, Eq.A13 is obtained.

$$\vec{\nabla}g = \hat{\theta}, \qquad \vec{\nabla}h = f_z\hat{r} - f_r\hat{z} \quad \text{(A13)}$$

In this case, special solutions can be found as in Eq.A14-15.

$$g_\theta = 1 \ \rightarrow g = \theta \ \rightarrow \ g(x,y,z) = \frac{y}{x} = V \qquad \text{(A14)}$$

$$h_r = f_z, \qquad h_z = -f_r, \qquad \rightarrow \frac{dz}{dr} = \frac{f_z}{f_r} \qquad \text{(A15)}$$

Eq.A14, as already guessed, turns out to be a plane that belongs to the rotational surface and rotates about the z-axis. So, given a family of surfaces of the form f(r,z)=U, g(x,y,z)=y/x. To find the remaining third family of orthogonal surfaces, a special solution satisfying the conditions in Eq. A15 will suffice. The integral constant that will appear in the last equation of Eq.A15 can be assigned as h.

Example 7:

Find the triple orthogonal coordinate surfaces to the surface family $f(x,y,x) = x^2 + y^2 + 2z^4 = U$.

Solution 7:

Since the given surface family is a rotational surface, g=y/x is known. To find the other surface family, h, we use Eq.A15.

$$f = r^2 + 2z^4, \qquad \frac{dz}{dr} = \frac{4z^3}{r}, \rightarrow dz z^{-3} = 4\frac{dr}{r} \ \rightarrow \ \frac{z^{-2}}{-2} = 4\ln r + c_1 \ \rightarrow$$
$$8\ln r + \frac{1}{z^2} = c_2 \ \rightarrow e^{\frac{1}{z^2}}(x^2+y^2)^4 = c_3 \qquad \text{(A16)}$$

As a result, the level surfaces shown in Eq.A16 form triple orthogonal coordinate systems.

$$f(x,y,x) = x^2 + y^2 + 2z^4 = U, \qquad g(x,y,z) = \frac{y}{x} = V,$$
$$h(x,y,z) = e^{\frac{1}{z^2}}(x^2+y^2)^4 = W \qquad \text{(A17)}$$

APPENDIX C

Verification of triple orthogonality of the level surfaces *f(x,y,z)=U, g(x,y,z)=V* and *h(x,y,z)=W* written in implicit form

```
close all; clear all; clc;
syms x y z A B u v x0 y0 z0 t p q

% For implicit Forms. Type the functions f, g, h
```

```
f=x^2+2*y^2+3*z^2; g=y/x^2; h=x^2+2*y^2-
(x0^2*(z/z0)^(2/3)+2*y0^2*(z/z0)^(4/3));

fx=diff(f,x); fy=diff(f,y); fz=diff(f,z); gx=diff(g,x); gy=diff(g,y); gz=diff(g,z);
hx=diff(h,x); hy=diff(h,y); hz=diff(h,z);
Dfg=simplify(fx*gx+fy*gy+fz*gz); Dfh=simplify(fx*hx+fy*hy+fz*hz);
Dgh=simplify(gx*hx+gy*hy+gz*hz);

% If "DotsParametric" and "DotsCartesian" are seen as [0, 0, 0], These surfaces are
orthogonal at (x0,y0,z0)
DotsParametric=[FG HF HG]
DotsCartesian=simplify([subs(Dfg,[x y z],[x0 y0 z0]) subs(Dfh,[x y z],[x0 y0 z0])
subs(Dgh,[x y z],[x0 y0 z0])],'IgnoreAnalyticConstraints',true)
```

APPENDIX D

Verification of triple orthogonality of the surfaces *F(u,v), G(u,v)* and *H(u,v)* written in parametric form

```
close all; clear all; clc;
syms x y z A B u v x0 y0 z0 t p q

% For parametric Forms. Type the parametric forms of the surfaces as F, G, H
F=simplify([sqrt(x0^2*exp(6*v)+4*u);sqrt(y0^2*exp(12*v)-
2*u);sqrt(x0^2+2*y0^2+3*z0^2-x0^2*exp(6*v)-
2*y0^2*exp(12*v))/sqrt(3)],'IgnoreAnalyticConstraints',true);
G=simplify([x0*exp(3*v)*exp(u);y0*exp(6*v)*exp(2*u);exp(u)*sqrt(x0^2+2*y0^2+
3*z0^2-x0^2*exp(6*v)-2*y0^2*exp(12*v))/sqrt(3)],'IgnoreAnalyticConstraints',true);
H=simplify([sqrt(x0^2*exp(2*v)+4*u);sqrt(y0^2*exp(4*v)-
2*u);z0*exp(3*v)],'IgnoreAnalyticConstraints',true);

Fu=simplify(diff(F,u),'IgnoreAnalyticConstraints',true);
Fv=simplify(diff(F,v),'IgnoreAnalyticConstraints',true);
Fn=simplify(cross(Fu,Fv),'IgnoreAnalyticConstraints',true);
Gu=simplify(diff(G,u),'IgnoreAnalyticConstraints',true);
Gv=simplify(diff(G,v),'IgnoreAnalyticConstraints',true);
Gn=simplify(cross(Gu,Gv),'IgnoreAnalyticConstraints',true);
```

```
Hu=simplify(diff(H,u),'IgnoreAnalyticConstraints',true);
Hv=simplify(diff(H,v),'IgnoreAnalyticConstraints',true);
Hn=simplify(cross(Hu,Hv),'IgnoreAnalyticConstraints',true);

dotFG=simplify(Gn(1)*Fn(1)+Gn(2)*Fn(2)+Gn(3)*Fn(3),'IgnoreAnalyticConstraints'
,true);
dotHG=simplify(Gn(1)*Hn(1)+Gn(2)*Hn(2)+Gn(3)*Hn(3),'IgnoreAnalyticConstraint
s',true);
dotHF=simplify(Fn(1)*Hn(1)+Fn(2)*Hn(2)+Fn(3)*Hn(3),'IgnoreAnalyticConstraints'
,true);

FG=simplify(subs(dotFG,[u v],[0 0]),'IgnoreAnalyticConstraints',true);
HG=simplify(subs(dotHG,[u v],[0 0]),'IgnoreAnalyticConstraints',true);
HF=simplify(subs(dotHF,[u v],[0 0]),'IgnoreAnalyticConstraints',true);
% If “DotsParametric” are seen as zero, the surfaces F, G, H are orthogonal
DotsParametric=[FG HF HG]
```

REFERENCES

Abdelmagid, A., Elshafei, A., Mansouri, M., & Hussein, A. (2022, September). A design model for a (grid) shell based on a triply orthogonal system of surfaces. In Design Modelling Symposium Berlin (pp. 46-60). Cham: Springer International Publishing.

Abdelmagid, A., Tošić, Z., Mirani, A., Hussein, A., & Elshafei, A. (2023). Design model for block-based structures from triply orthogonal systems of surfaces. In Advances in Architectural Geometry 2023 (pp. 165-176). De Gruyter.

Bae, S. H., & Choi, B. K. (2002). NURBS surface fitting using orthogonal coordinate transform for rapid product development. Computer-Aided Design, 34(10), 683-690.

Bobenko, A. I., Matthes, D., & Suris, Y. B. (2003). Discrete and smooth orthogonal systems: C∞-approximation. International Mathematics Research Notices, 2003(45), 2415-2459.

Cayley, A. (1872). Sur la condition pour qu'une famille de surfaces données puisse faire partie d'un système orthogonal. CR Académie des Sciences, Paris, 75, 177-185.

Cayley, A. (1873). On curvature and orthogonal surfaces. Philosophical Transactions of the Royal Society of London, 163, 229-251.

Colapinto, P. (2016). Articulating space: geometric algebra for parametric design-symmetry, kinematics, and curvature. University of California, Santa Barbara.

Colapinto, P. (2017). Composing surfaces with conformal rotors. Advances in Applied Clifford Algebras, 27, 453-474.

Darboux, G. (1910). Leçons sur les systèmes orthogonaux et les coordonnées curvilignes. Gauthier-Villars.

Eisenhart, L. P. (1907). Certain triply orthogonal systems of surfaces. American Journal of Mathematics, 29(2), 168-212.

Ferréol, R. (2017). Triple orthogonal surfaces. Retrieved from https://mathcurve.com/surfaces.gb/tripleorthogonal/tripleorthog.shtml

Finat, J. (n.d.). Extrinsic geometry of surfaces. Unpublished manuscript.

Garcia, R. O. N. A. L. D. O., & Tejada, D. (2023). Principal lines on an ellipsoid in a Minkowski tridimensional space. arXiv preprint arXiv:2306.07979.

Hester, E. W., & Vasil, G. M. (2023). Orthogonal signed-distance coordinates and vector calculus near evolving curves and surfaces. Proceedings of the Royal Society A, 479(2277), 20230080.

Hoque, M. F., Kubů, O., Marchesiello, A., & Šnobl, L. (2023). New classes of quadratically integrable systems with velocity-dependent potentials: non-subgroup type cases. The European Physical Journal Plus, 138(9), 845.

Hotine, M. (1966). Triply orthogonal coordinate systems. Bulletin Géodésique, 81, 195-224.

Ivers, D. J. (2017). Kinematic dynamos in spheroidal geometries. Proceedings of the Royal Society A, 473(2206), 20170432.

Kasner, E. (1909). Natural families of trajectories: conservative fields of force. Transactions of the American Mathematical Society, 10(2), 201-219.

Kasner, E. (1911). Natural systems of trajectories generating families of Lamé. Transactions of the American Mathematical Society, 70-74.

Kubů, O., Marchesiello, A., & Šnobl, L. (2023). New classes of quadratically integrable systems in magnetic fields: the generalized cylindrical and spherical cases. Annals of Physics, 451, 169264.

Lester, D. R., Dentz, M., Bandopadhyay, A., & Le Borgne, T. (2022). Fluid deformation in isotropic Darcy flow. Journal of Fluid Mechanics, 945, A18.

Malits, P., Haridim, M., & Chulski, S. (2015). TEM wave propagation in a microstrip line on a substrate of circular segment cross section. Zeitschrift für angewandte Mathematik und Physik, 66, 3727-3735.

Menjanahary, J. M., Hoxhaj, E., & Krasauskas, R. (2024). Classification of Dupin cyclidic cubes by their singularities. Computer Aided Geometric Design, 102362.

Panou, G. C. (2014). A study on geodetic boundary value problems in ellipsoidal geometry.

Panou, G., Korakitis, R., & Delikaraoglou, D. (2016). Triaxial coordinate systems and their geometrical interpretation. Measuring and Mapping the Earth. Ziti Editions, Thessaloniki, Greece, 126-135.

Ricci, R. J. (1976). SPACEBAR: Kinematic design by computer graphics. Computer-Aided Design, 8(4), 219-226.

Ryskin, G., & Leal, L. G. (1983). Orthogonal mapping. Journal of Computational Physics, 50(1), 71-100.

Sizykh, G. B. (2020). System of orthogonal curvilinear coordinates on the isentropic surface behind a detached bow shock wave. Fluid Dynamics, 55, 899-903.

Smith, W. D. (2004). On the finiteness and shape of the universe.

Strunz, P. (2023). Unit vectors for similar oblate spheroidal coordinates and vector transformation. Zeitschrift für angewandte Mathematik und Physik, 74(5), 172.

Viaggiu, S. (2018). An algorithm to generate anisotropic rotating fluids with vanishing viscosity. The European Physical Journal Plus, 133(12), 551.

Weatherburn, C. E. (1926). On Lamé families of surfaces. Annals of Mathematics, 28(1/4), 301-308.

Wright, J. E. (1906). An application of the theory of differential invariants to triply orthogonal systems of surfaces.

Zakharov, V. E. (1998). Description of the n-orthogonal curvilinear coordinate systems and Hamiltonian integrable systems of hydrodynamic type, I: Integration of the Lamé equations.

Zund, J. D., & Moore, W. (1987). Hotine's conjecture in differential geodesy. Bulletin Géodésique, 61, 209-222.

CHAPTER 2

THE MATRIX REPRESENTATIONS AND IDENTITIES OF THE COMPLEX GENERALIZED k-FIBONACCI NUMBERS

Assoc. Prof. Dr. Kübra GÜL[1]

DOI: https://www.doi.org/10.5281/zenodo.18077808

[1] Department of Computer Engineering, Kafkas University, Kars, Turkey. kubra.gullb@gmail.com, orcid id: 0000-0002-8732-5718

1. INTRODUCTION

The Fibonacci sequence and its various generalizations hold an important place in both classical number theory and modern algebra (Koshy, 2017). The k-Fibonacci and k-Lucas sequences introduced by Falcon and Plaza (Falcon, 2011; Falcon & Plaza, 2007) were studied and extended in many areas, including combinatorics, linear algebra, and applied sciences. In addition to these developments, matrix-based approaches have played a central role in understanding generalized Fibonacci structures. Notably, Kumar and Sahani (Kumar & Sahani, 2025) provided a comprehensive treatment of the generalized k-Fibonacci sequence using the Q-matrix framework, while the authors (Ahmad & Prasher, 2022) introduced the matrix representations that further expanded the matrix interpretation of such sequences. These foundational studies demonstrate that many properties and identities of generalized Fibonacci sequences can be derived systematically through matrix powers and determinant relations. Moreover, many researchers have shown that Fibonacci-type sequences exhibit a richer and more flexible algebraic structure when extended to broader number systems such as complex, dual, bicomplex, and quaternionic algebras (Berzsenyi, 1975; Gül, 2020; Harman, 1981; Horadam, 1963; Prasad, 2021).

In this context, the complex generalized k-Fibonacci numbers (CGFs) provide a natural extension of the classical k-Fibonacci numbers into the complex plane. The close relationship between the CGFs and the k-Fibonacci matrices makes matrix representations a powerful tool for studying their structural and algebraic properties. This approach allows many identities and transformations associated with the sequence to be obtained systematically. Matrix methods have long been used as an effective technique in the analysis of Fibonacci-type sequences. In particular, powers of the classical Q-matrix provide closed-form expressions and essential structural insights. In the study of the CGFs, both the Q-matrix and the P-matrix, which describes even-indexed terms, are employed, while the matrix H plays a key role in revealing further structural features.

This section presents the matrix representations in detail and, by using the Binet-type formula, derives several fundamental identities such as the Cassini, Catalan, and Vajda identities. In this way, it demonstrates that the complex generalized k-Fibonacci sequence can be generated through matrix

methods and that its fundamental algebraic identities emerge naturally within this framework.

The k-Fibonacci numbers are defined by the recurrence

$$F_{k,n} = kF_{k,n-1} + F_{k,n-2}, \qquad n \geq 2,$$

where the initial values are specified as $F_{k,0} = 0, F_{k,1} = 1$ (Falcon & Plaza, 2007).

Let k be any positive real number and let p and q be positive integers. The generalized k-Fibonacci numbers introduced in (Panwar, 2021) are defined by

$$\mathcal{F}_{k,n} = pk\mathcal{F}_{k,n-1} + q\mathcal{F}_{k,n-2}, \qquad n \geq 2,$$

with initial values $\mathcal{F}_{k,0} = a, \mathcal{F}_{k,1} = b$.

For a positive real number k and a fixed positive integer m, the generalized k-Fibonacci numbers are defined by

$$Q_{k,n} = kQ_{k,n-1} + Q_{k,n-2}, \qquad n \geq 2,$$

where the initial values are $Q_{k,0} = m$, $Q_{k,1} = km$.

The complex Fibonacci numbers are defined by

$$F_n^{\,*} = F_n + iF_{n+1}, \qquad n \geq 0,$$

where $\sqrt{-1} = i$ and F_n is the n-th Fibonacci number (Horadam, 1961).

2. MAIN RESULTS

Definition 2.1. Let m be a given positive integer. For $n \geq 0$, the complex generalized k-Fibonacci numbers (denoted by CGFs) are defined as follows:

$$\mathcal{C}_{k,n} = Q_{k,n} + iQ_{k,n+1}$$

with initial conditions $\mathcal{C}_{k,0} = m(1 + ki), \mathcal{C}_{k,1} = km + i(m + k^2m)$.

Note that, for $n \geq 0$, there is the following recurrence relation:

$$\mathcal{C}_{k,n+2} = k\mathcal{C}_{k,n+1} + \mathcal{C}_{k,n}.$$

One of the most known Fibonacci matrices (Gould, 1981; Hoggatt, 1969) is the matrix Q_1 which is defined by

$$Q_1 = \begin{bmatrix} 1 & 1 \\ 1 & 0 \end{bmatrix}$$

such that

$$Q_1^n = \begin{bmatrix} F_{n+1} & F_n \\ F_n & F_{n-1} \end{bmatrix}.$$

The two matrix representations of the CGFs are given by

$$Q = \begin{bmatrix} k & 1 \\ 1 & 0 \end{bmatrix} \text{ and } P = \begin{bmatrix} k^2+1 & k \\ k & 1 \end{bmatrix}.$$

For a positive integer n, the corresponding matrix form is given by:

$$\begin{bmatrix} \mathcal{C}_{k,n+1} \\ \mathcal{C}_{k,n} \end{bmatrix} = \begin{bmatrix} k & 1 \\ 1 & 0 \end{bmatrix} \begin{bmatrix} \mathcal{C}_{k,n} \\ \mathcal{C}_{k,n-1} \end{bmatrix}.$$

Now, let us define the following matrix called Q-matrix based on the complex generalized k-Fibonacci numbers

$$Q_{\mathcal{C}}^{(k,n)} = \begin{bmatrix} \mathcal{C}_{k,n} & \mathcal{C}_{k,n-1} \\ \mathcal{C}_{k,n-1} & \mathcal{C}_{k,n-2} \end{bmatrix}$$

with the entries $\mathcal{C}_{k,n}$. Considering the matrix $H = \begin{bmatrix} 1+ik & i \\ i & 1 \end{bmatrix}$, it is clearly seen that

$$Q_{\mathcal{C}}^{(k,n)} = mHQ^n,$$

where $Q^n = m^{-1}\begin{bmatrix} Q_{k,n} & Q_{k,n-1} \\ Q_{k,n-1} & Q_{k,n-2} \end{bmatrix}$.

Theorem 2.1. For any positive integer n, the following relation holds:

$$\begin{bmatrix} \mathcal{C}_{k,n+1} \\ \mathcal{C}_{k,n} \end{bmatrix} = Q^n \begin{bmatrix} \mathcal{C}_{k,1} \\ \mathcal{C}_{k,0} \end{bmatrix}.$$

Proof. We establish the result by mathematical induction on n. For the base case $n = 1$, the statement follows immediately. Assume now that the formula holds for some integer n. Under this assumption, it remains to verify that the identity is also valid for $n + 1$.

$$\begin{bmatrix} k & 1 \\ 1 & 0 \end{bmatrix}^{n+1} \begin{bmatrix} 1+ik & i \\ i & 1 \end{bmatrix} \begin{bmatrix} Q_{k,1} \\ Q_{k,0} \end{bmatrix} = \begin{bmatrix} k & 1 \\ 1 & 0 \end{bmatrix} \begin{bmatrix} k & 1 \\ 1 & 0 \end{bmatrix}^{n} \begin{bmatrix} 1+ik & i \\ i & 1 \end{bmatrix} \begin{bmatrix} Q_{k,1} \\ Q_{k,0} \end{bmatrix}$$

$$= \begin{bmatrix} k & 1 \\ 1 & 0 \end{bmatrix} \begin{bmatrix} \mathcal{C}_{k,n+1} \\ \mathcal{C}_{k,n} \end{bmatrix} = \begin{bmatrix} \mathcal{C}_{k,n+2} \\ \mathcal{C}_{k,n+1} \end{bmatrix}.$$

Theorem 2.2. For integers $n, r \geq 1$, the following identity holds:

$$m\mathcal{C}_{k,n+r} = \left(Q_{k,n}\mathcal{C}_{k,r} + Q_{k,n-1}\mathcal{C}_{k,r-1}\right).$$

Proof. We know that

$$HQ^{n+r} = m^{-1}\begin{bmatrix} \mathcal{C}_{k,n+r} & \mathcal{C}_{k,n+r-1} \\ \mathcal{C}_{k,n+r-1} & \mathcal{C}_{k,n+r-2} \end{bmatrix}.$$

Since $Q^{n+r} = Q^n Q^r$, we obtain

$$HQ^{n+r} = Q^n(HQ^r).$$

Hence,

$$\begin{bmatrix} \mathcal{C}_{k,n+r} & \mathcal{C}_{k,n+r-1} \\ \mathcal{C}_{k,n+r-1} & \mathcal{C}_{k,n+r-2} \end{bmatrix} = m^{-1} \begin{bmatrix} Q_{k,n} & Q_{k,n-1} \\ Q_{k,n-1} & Q_{k,n-2} \end{bmatrix} \begin{bmatrix} \mathcal{C}_{k,r} & \mathcal{C}_{k,r-1} \\ \mathcal{C}_{k,r-1} & \mathcal{C}_{k,r-2} \end{bmatrix}.$$

By comparing the entries in the first row and first column on both sides, we have

$$m\mathcal{C}_{k,n+r} = \left(Q_{k,n}\mathcal{C}_{k,r} + Q_{k,n-1}\mathcal{C}_{k,r-1}\right).$$

Theorem 2.3. For integers $n, r \geq 1$, the following identity holds:

$$m(2i-k)Q_{k,n+r} = \mathcal{C}_{k,n}\mathcal{C}_{k,r-1} + \mathcal{C}_{k,n-1}\mathcal{C}_{k,r-2}.$$

Proof. Since $HQ^n = Q^nH$, we now demonstrate that

$$H(Q^{n+r}H) = (Q^nH)(Q^rH),$$

$$H(Q^{n+r}H) = m^{-1}\begin{bmatrix} 1+ik & i \\ i & 1 \end{bmatrix}\begin{bmatrix} \mathcal{C}_{k,n+r} & \mathcal{C}_{k,n+r-1} \\ \mathcal{C}_{k,n+r-1} & \mathcal{C}_{k,n+r-2} \end{bmatrix}$$

$$= m^{-1}(2i-k)\begin{bmatrix} Q_{k,n+r+1} & Q_{k,n+r} \\ Q_{k,n+r} & Q_{k,n+r-1} \end{bmatrix},$$

$$(Q^nH)(Q^rH) = m^{-2}\begin{bmatrix} \mathcal{C}_{k,n} & \mathcal{C}_{k,n-1} \\ \mathcal{C}_{k,n-1} & \mathcal{C}_{k,n-2} \end{bmatrix}\begin{bmatrix} \mathcal{C}_{k,r} & \mathcal{C}_{k,r-1} \\ \mathcal{C}_{k,r-1} & \mathcal{C}_{k,r-2} \end{bmatrix}.$$

$$(2i-k)\begin{bmatrix} Q_{k,n+r+1} & Q_{k,n+r} \\ Q_{k,n+r} & Q_{k,n+r-1} \end{bmatrix} = m^{-1}\begin{bmatrix} \mathcal{C}_{k,n} & \mathcal{C}_{k,n-1} \\ \mathcal{C}_{k,n-1} & \mathcal{C}_{k,n-2} \end{bmatrix}\begin{bmatrix} \mathcal{C}_{k,r} & \mathcal{C}_{k,r-1} \\ \mathcal{C}_{k,r-1} & \mathcal{C}_{k,r-2} \end{bmatrix}.$$

Inspection of the first row and second column entries on each side shows that

$$m(2i-k)Q_{k,n+r} = \mathcal{C}_{k,n}\mathcal{C}_{k,r-1} + \mathcal{C}_{k,n-1}\mathcal{C}_{k,r-2}.$$

Theorem 2.4. The Cassini's identity for the CGFs is as follows:

$$\mathcal{C}_{k,n+1}\mathcal{C}_{k,n-1} - \mathcal{C}_{k,n}^2 = (2+ik)(-1)^{n+1}m^2.$$

Proof. In (Soykan, 2019), it is known that $\begin{vmatrix} F_{k,n+1} & F_{k,n} \\ F_{k,n} & F_{k,n-1} \end{vmatrix} = (-1)^n$. Similarly, $Q = \begin{bmatrix} k & 1 \\ 1 & 0 \end{bmatrix}$, $|Q^n| = (-1)^n$. Moreover, for the matrix $Q_{\mathcal{C}}^{(k,n)}$, we have

$$\left|Q_{\mathcal{C}}^{(k,n)}\right| = |mHQ^n| = m^2\left(\mathcal{C}_{k,n}\mathcal{C}_{k,n-2} - \mathcal{C}_{k,n-1}^2\right).$$

On the other hand, since $|H| = 2 + ik$, it follows that

$$\left|Q_{\mathcal{C}}^{(k,n)}\right| = m^2(2+ik)(-1)^n.$$

Hence

$$m^2(2+ik)(-1)^n = \left(\mathcal{C}_{k,n}\mathcal{C}_{k,n-2} - \mathcal{C}_{k,n-1}^2\right).$$

Finally, replacing n by $n+1$ in the above relation, we obtain

$$\mathcal{C}_{k,n+1}\mathcal{C}_{k,n-1} - \mathcal{C}_{k,n}^2 = m^2(2+ik)(-1)^{n+1},$$

which completes the proof.

For the matrix representation P of the CGFs, $P^n = m^{-1}\begin{bmatrix} Q_{k,2n} & Q_{k,2n-1} \\ Q_{k,2n-1} & Q_{k,2n-2} \end{bmatrix}$.

Then we have

$$Q_{\mathcal{C}}^{(k,2n)} = mHP^n.$$

Theorem 2.5. For any positive integer n, we obtain

$$\begin{bmatrix} \mathcal{C}_{k,2n+1} \\ \mathcal{C}_{k,2n} \end{bmatrix} = \begin{bmatrix} k^2+1 & k \\ k & 1 \end{bmatrix}\begin{bmatrix} \mathcal{C}_{k,2n-1} \\ \mathcal{C}_{k,2n-2} \end{bmatrix}.$$

Proof. Using the recurrence relation of the CGFs, we have

$$\begin{bmatrix} \mathcal{C}_{k,2n+1} \\ \mathcal{C}_{k,2n} \end{bmatrix} = \begin{bmatrix} k\left(k\mathcal{C}_{k,2n-1} + \mathcal{C}_{k,2n-2}\right) + \mathcal{C}_{k,2n-1} \\ k\mathcal{C}_{k,2n-1} + \mathcal{C}_{k,2n-2} \end{bmatrix}$$

$$= \begin{bmatrix} k^2+1 & k \\ k & 1 \end{bmatrix}\begin{bmatrix} \mathcal{C}_{k,2n-1} \\ \mathcal{C}_{k,2n-2} \end{bmatrix}.$$

Theorem 2.6. The Cassini-like identity for the CGFs is as follows:

$$\mathcal{C}_{k,2n}\mathcal{C}_{k,2n-2} - \mathcal{C}_{k,2n-1}^2 = m^2(2+ik).$$

Proof. For the matrix

$$Q_{\mathcal{C}}^{(k,n)} = \begin{bmatrix} \mathcal{C}_{k,n} & \mathcal{C}_{k,n-1} \\ \mathcal{C}_{k,n-1} & \mathcal{C}_{k,n-2} \end{bmatrix},$$

Recall that

$$\left|Q_{\mathcal{C}}^{(k,2n)}\right| = |mHP^n|$$

where $H = \begin{bmatrix} 1+ik & i \\ i & 1 \end{bmatrix}$, $P = Q^2 = \begin{bmatrix} k^2+1 & k \\ k & 1 \end{bmatrix}$.

Hence,

$$\left(\mathcal{C}_{k,2n}\mathcal{C}_{k,2n-2} - \mathcal{C}_{k,2n-1}^2\right) = m^2|H||P^n|.$$

Then, this yields

$$\mathcal{C}_{k,2n}\mathcal{C}_{k,2n-2} - \mathcal{C}_{k,2n-1}^2 = m^2(2+ik),$$

which completes the proof.

Theorem 2.7. For the integers n and r, we have

$$m\left(\mathcal{C}_{k,2n+2r} + i\mathcal{C}_{k,2n+2r+1}\right) = \mathcal{C}_{k,2n}\mathcal{C}_{k,2r} + \mathcal{C}_{k,2n-1}\mathcal{C}_{k,2r-1}.$$

Proof. Since $HP^n = P^nH$, we now demonstrate that

$$H(P^{n+r}H) = (P^nH)(P^rH),$$

$$H(P^{n+r}H) = m^{-1}\begin{bmatrix}1+ik & i\\ i & 1\end{bmatrix}\begin{bmatrix}\mathcal{C}_{k,2n+2r} & \mathcal{C}_{k,2n+2r-1}\\ \mathcal{C}_{k,2n+2r-1} & \mathcal{C}_{k,2n+2r-2}\end{bmatrix}$$
$$= m^{-1}(2i-k)\begin{bmatrix}Q_{k,2n+2r+1} & Q_{k,2n+2r}\\ Q_{k,2n+2r} & Q_{k,2n+2r-1}\end{bmatrix},$$
$$(P^nH)(P^rH) = m^{-2}\begin{bmatrix}\mathcal{C}_{k,2n} & \mathcal{C}_{k,2n-1}\\ \mathcal{C}_{k,2n-1} & \mathcal{C}_{k,2n-2}\end{bmatrix}\begin{bmatrix}\mathcal{C}_{k,2r} & \mathcal{C}_{k,2r-1}\\ \mathcal{C}_{k,2r-1} & \mathcal{C}_{k,2r-2}\end{bmatrix}$$
$$= m^{-2}(2i-k)\begin{bmatrix}Q_{k,2n+2r+1} & Q_{k,2n+2r}\\ Q_{k,2n+2r} & Q_{k,2n+2r-1}\end{bmatrix},$$

Since $H(P^{n+r}H) = (P^nH)(P^rH)$, we can write

$$\begin{bmatrix}1+ik & i\\ i & 1\end{bmatrix}\begin{bmatrix}\mathcal{C}_{k,2n+2r} & \mathcal{C}_{k,2n+2r-1}\\ \mathcal{C}_{k,2n+2r-1} & \mathcal{C}_{k,2n+2r-2}\end{bmatrix} = m^{-1}\begin{bmatrix}\mathcal{C}_{k,2n} & \mathcal{C}_{k,2n-1}\\ \mathcal{C}_{k,2n-1} & \mathcal{C}_{k,2n-2}\end{bmatrix}\begin{bmatrix}\mathcal{C}_{k,2r} & \mathcal{C}_{k,2r-1}\\ \mathcal{C}_{k,2r-1} & \mathcal{C}_{k,2r-2}\end{bmatrix}.$$

Equating the first row and column element in both sides of the equation, we have

$$m\left(\mathcal{C}_{k,2n+2r} + i\mathcal{C}_{k,2n+2r+1}\right) = \mathcal{C}_{k,2n}\mathcal{C}_{k,2r} + \mathcal{C}_{k,2n-1}\mathcal{C}_{k,2r-1}.$$

Theorem 2.8. Whenever n and r are integers, the following relations hold:

$$m\mathcal{C}_{k,2n+2r} = Q_{k,2n}\mathcal{C}_{k,2r} + Q_{k,2n-1}\mathcal{C}_{k,2r-1},$$
$$m\mathcal{C}_{k,2n+2r-1} = Q_{k,2n}\mathcal{C}_{k,2r-1} + Q_{k,2n-1}\mathcal{C}_{k,2r-2}.$$

Proof. By the previously obtained expression, we have

$$HP^{n+r} = m^{-1}\begin{bmatrix}\mathcal{C}_{k,2n+2r} & \mathcal{C}_{k,2n+2r-1}\\ \mathcal{C}_{k,2n+2r-1} & \mathcal{C}_{k,2n+2r-2}\end{bmatrix}.$$

Since $P^{n+r} = P^nP^r$, we obtain

$$HP^{n+r} = P^n(HP^r).$$

Hence,

$$m^{-1}\begin{bmatrix}\mathcal{C}_{k,2n+2r} & \mathcal{C}_{k,2n+2r-1}\\ \mathcal{C}_{k,2n+2r-1} & \mathcal{C}_{k,2n+2r-2}\end{bmatrix} = m^{-2}\begin{bmatrix}Q_{k,2n} & Q_{k,2n-1}\\ Q_{k,2n-1} & Q_{k,2n-2}\end{bmatrix}\begin{bmatrix}\mathcal{C}_{k,2r} & \mathcal{C}_{k,2r-1}\\ \mathcal{C}_{k,2r-1} & \mathcal{C}_{k,2r-2}\end{bmatrix}.$$

By comparing the (1,1)-entries of the matrices on both sides, we obtain

$$m\mathcal{C}_{k,2n+2r} = \left(Q_{k,2n}\mathcal{C}_{k,2r} + Q_{k,2n-1}\mathcal{C}_{k,2r-1}\right).$$

In the same manner, examining the (1,2)-entries yields

$$m\mathcal{C}_{k,2n+2r-1} = Q_{k,2n}\mathcal{C}_{k,2r-1} + Q_{k,2n-1}\mathcal{C}_{k,2r-2}.$$

An explicit representation of the complex generalized k-Fibonacci numbers can be obtained by analyzing the characteristic roots of their recurrence relation. This procedure leads directly to a closed-form expression for $\mathcal{C}_{k,n}$.

$$\mathcal{C}_{k,n} = \frac{\hat{p}p^n - \hat{q}q^n}{p-q}$$

where $p = \frac{k+\sqrt{k^2+4}}{2}$, $q = \frac{k-\sqrt{k^2+4}}{2}$, $\hat{p} = m((1+ik)p + i)$ and $\hat{q} = m((1+ik)q + i)$.

Theorem 2.9. The sum of the first $n+1$ terms of the complex generalized k-Fibonacci sequence is given by

$$\sum_{j=0}^{n} \mathcal{C}_{k,j} = \frac{\mathcal{C}_{k,n+2} - (k-1)\mathcal{C}_{k,n+1} + (k-1)\mathcal{C}_{k,0} - \mathcal{C}_{k,1}}{k}.$$

Proof. Using the recurrence relation

$$\mathcal{C}_{k,n+2} = k\mathcal{C}_{k,n+1} + \mathcal{C}_{k,n} \qquad n \geq 0,$$

we can rewrite the initial terms as

$$\mathcal{C}_{k,0} = \mathcal{C}_{k,2} - k\mathcal{C}_{k,1},$$
$$\mathcal{C}_{k,1} = \mathcal{C}_{k,3} - k\mathcal{C}_{k,2},$$
$$\mathcal{C}_{k,2} = \mathcal{C}_{k,4} - k\mathcal{C}_{k,3},$$

and continuing in the same manner, we can generalize this pattern to

$$\mathcal{C}_{k,j} = \mathcal{C}_{k,j+2} - k\mathcal{C}_{k,j+1},$$

for $0 \leq j \leq n$. Then, as a result of necessary calculations, we get

$$\sum_{j=0}^{n} \mathcal{C}_{k,j} = \frac{\mathcal{C}_{k,n+2} - (k-1)\mathcal{C}_{k,n+1} + (k-1)\mathcal{C}_{k,0} - \mathcal{C}_{k,1}}{k}.$$

Lemma 2.1. The following identity is satisfied:

$$\hat{p}\hat{q} = -m^2(2+ik).$$

Proof. Because $\hat{p}$ and $\hat{q}$ are defined using the characteristic roots, their product simplifies easily and the identity follows directly.

$$\begin{aligned}\hat{p}\hat{q} &= m^2(-2 - 2ik + i(p+q) + k^2 - k(p+q)) \\ &= m^2(-2(1+ik) + (i-k)k + k^2) \\ &= -m^2(2+ik).\end{aligned}$$

Theorem 2.10. Vajda's identity for the CGFs is as follows:

$$\mathcal{C}_{k,n+r}\mathcal{C}_{k,n+s} - \mathcal{C}_{k,n}\mathcal{C}_{k,n+r+s} = (-1)^{n+1}m^2(2+ik)F_{k,r}F_{k,s},$$

where $F_{k,n}$ is the nth k-Fibonacci number.

Proof. Using the Binet-type formula for the CGFs, we obtain

$$\mathcal{C}_{k,n+r}\mathcal{C}_{k,n+s} - \mathcal{C}_{k,n}\mathcal{C}_{k,n+r+s} = \frac{\hat{p}p^{n+r} - \hat{q}q^{n+r}}{p-q}\frac{\hat{p}p^{n+s} - \hat{q}q^{n+s}}{p-q} - \frac{\hat{p}p^{n} - \hat{q}q^{n}}{p-q}\frac{\hat{p}p^{n+r+s} - \hat{q}q^{n+r+s}}{p-q}$$

$$= \frac{\hat{p}^2 p^{2n+r+s} - \hat{p}\hat{q}(p^{n+s}q^{n+r} + q^{n+s}p^{n+r}) + \hat{q}^2 q^{2n+s+r}}{(p-q)^2}$$
$$- \frac{\hat{p}^2 p^{2n+r+s} - \hat{p}\hat{q}(p^{n}q^{n+r+s} + q^{n}p^{n+r+s}) + \hat{q}^2 q^{2n+r+s}}{(p-q)^2}$$
$$= \frac{\hat{p}\hat{q}(pq)^n(-p^s q^r - q^s p^r + q^{r+s} + p^{r+s})}{(p-q)^2}$$
$$= \frac{\hat{p}\hat{q}(-1)^n(p^r - q^r)(p^s - q^s)}{(p-q)^2}$$
$$= (-1)^n \hat{p}\hat{q} F_{k,r} F_{k,s}$$
$$= (-1)^{n+1} m^2 (2 + ik) F_{k,r} F_{k,s}.$$

Corollary 2.1. Cassini's identity for the CGFs is as follows:

$$\mathcal{C}_{k,n+1}\mathcal{C}_{k,n-1} - \mathcal{C}_{k,n}^2 = m^2(2 + ik)(-1)^{n+1} F_{k,1} F_{k,-1}.$$

Proof. The result follows directly by taking $r = -s = 1$ in Vajda's identity.

Corollary 2.2. Catalan's identity for the CGFs is as follows:

$$\mathcal{C}_{k,n+r}\mathcal{C}_{k,n-r} - \mathcal{C}_{k,n}^2 = m^2(2 + ik)(-1)^{n+1} F_{k,r} F_{k,-r}.$$

Proof. By replacing s with $-r$ in Vajda's identity gives the Catalan identity for the CGFs.

CONCLUSION

In this study, the complex generalized k-Fibonacci numbers (CGFs) were investigated through matrix representations and the Binet-type formula. It was shown that the matrices Q, P, and H generate the sequence and reveal its fundamental properties. Through this approach, Cassini, Catalan, and Vajda identities for the CGFs were obtained, and additional identities involving even-indexed terms were derived. The results demonstrate that the CGFs preserve the structure of the classical Fibonacci numbers while extending it into the complex plane with a richer algebraic framework. It is concluded that the matrix-based methods used here have potential applications to other generalized Fibonacci-type sequences and related algebraic systems.

REFERENCES

Ahmad, N., & Prasher, L. (2022). Q1 and Q2 Matrix Representations of Generalized K-Fibonacci Sequence. JP Journal of Algebra, Number Theory and Applications, 54,19–34. https://doi.org/10.17654/0972555522013

Berzsenyi, G. (1975). Sums of products of generalized Fibonacci numbers. Fibonacci Quarterly, 13, 343–344.

Falcon, S. (2011). On the k-Lucas numbers. International Journal of Contemporary Mathematical Sciences, 6(21), 1039–1050.

Falcon, S., & Plaza, A. (2007). On the k-Fibonacci numbers. Chaos, Solitons & Fractals, 32(5), 1615–1624.

Gould, H. W. (1981). A history of the Fibonacci Q-matrix and a higher-dimensional problem. The Fibonacci Quarterly, 19(3), 250–257. https://doi.org/10.1080/00150517.1981.12430088

Gül, K. (2020). Dual bicomplex Horadam quaternions. Notes on Number Theory and Discrete Mathematics, 26(4), 187–205. https://doi.org/10.7546/nntdm.2020.26.4.187-205

Harman, C. J. (1981). Complex Fibonacci numbers. The Fibonacci Quarterly, 19(1), 82–86.

Hoggatt, V. E. (1969). Fibonacci and Lucas numbers. Houghton-Mifflin.

Horadam, A. F. (1961). A generalized Fibonacci sequence. American Mathematical Monthly, 69, 455–459. https://doi.org/10.1080/00029890.1961.11989696

Horadam, A. F. (1963). Complex Fibonacci numbers and Fibonacci quaternions. American Mathematical Monthly, 70(3), 289–291. https://doi.org/10.2307/2313129

Koshy, T. (2017). Fibonacci and Lucas numbers with applications. John Wiley & Sons. https://doi.org/10.1002/9781118742327

Kumar, N. K., & Sahani, S. K. (2025). Generalized k-Fibonacci Sequence of Q-Matrix. Mikailalsys Journal of Advanced Engineering International, 2(1), 55-62. https://doi.org/10.58578/mjaei.v2i1.4811

Panwar, Y. (2021). A note on the generalized k-Fibonacci sequence. Naturengs, 2, 29–39. https://doi.org/10.46572/naturengs.937010

Prasad, B. (2021). Dual complex Fibonacci p-numbers. Chaos, Solitons & Fractals, 145, 109922. . https://doi.org/10.1016/j.chaos.2020.109922

Soykan, Y. (2019). Simson identity of generalized m-step Fibonacci numbers. International Journal of Advances in Applied Mathematics and Mechanics, 7(2), 45–56.

CHAPTER 3

REAL-TIME ESTIMATION OF RAT TUMORS USING EXTENDED KALMAN FILTER VARIANTS IN A LINEAR DYNAMICAL FRAMEWORK

Assoc. Prof. Dr. Levent ÖZBEK[1]

DOI: https://www.doi.org/10.5281/zenodo.18077823

[1] Ankara University, Faculty of Science, Department of Statistics, Ankara, Türkiye. ozbek@science.ankara.edu.tr, orcid id:000-0003-1018-3114

1. INTRODUCTION

Compartment models are useful for describing ICG pharmacokinetics, but they struggle with rapid or nonlinear changes common in tumor tissue. To address this, we use a state-space approach and evaluate four Extended Kalman Filter (EKF) variants—standard, Adaptive-R, Forgetting Factor, and Mahalanobis Distance—on real ICG data from tumor-bearing subjects. We further introduce a three-dimensional state formulation that includes concentration, velocity, and acceleration, enabling more sensitive detection of vascular transitions such as changes in permeability or perfusion. This enriched framework improves real-time estimation accuracy and enhances physiological interpretability of tumor microvascular dynamics.

2. ESTIMATION METHODOLOGY

The Kalman Filter (KF) provides an optimal recursive method for estimating the states of linear systems under Gaussian noise and is widely used in engineering and biomedical applications. Because biological systems often exhibit nonlinear behavior, the Extended Kalman Filter (EKF) is employed by linearizing the dynamics around the current estimate. In pharmacokinetics, indocyanine green (ICG) dynamics in tumor tissue show nonlinearities driven by heterogeneous perfusion and variable permeability. To better capture these effects, we use a three-dimensional state-space model that includes concentration, velocity, and acceleration—parameters that reveal rapid uptake or clearance and higher-order vascular transitions. We compare four EKF variants—standard, Adaptive-R, Forgetting Factor, and Mahalanobis Distance—on real ICG data from tumor-bearing animals. These recursive filters enable real-time estimation without offline curve fitting and offer improved temporal resolution, robustness to noise, and sensitivity to transient physiological changes, providing a powerful framework for dynamic tissue characterization [1-11].

2.1 State-space model and AKF

Given a general discrete-time stochastic system described by its state and observation equations,

$$x_k = F_k x_{k-1} + w_{k-1} \tag{1}$$

$$y_k = H_k x_{k-1} + v_{k-1} \tag{2}$$

where x_k is an $n\times1$ system, y_k is an $m\times1$ observation vector, F_k is an $n\times n$ system, H_k is an observation $m\times n$ matrix, The covariance matrices w_t and v_t are defined by $w_k \sim N(0,Q_k)$ and $v_k \sim N(0,R_k)$. Let the initial state be assumed to have a Gaussian distribution in the form of $x_0 \sim N(\bar{x}_0, P_0)$. The optimum update equations for KF are

$$\hat{x}_{k|k} = \hat{x}_{k-1|k-1} + K_k n_k \tag{3}$$

$$P_{k|k-1} = F_k P_{k-1|k-1} F_k' + Q_k \tag{4}$$

$$n_k = z_k - h_k(\hat{x}_{k|k-1}) \tag{5}$$

$$S_k = H_k P_{k|k-1} H_k' + R_k \tag{6}$$

$$K_k = P_{k|k-1} H_k' S_k^{-1} \tag{7}$$

$$P_{k|k} = (I - K_k H_k) P_{k|k-1} \tag{8}$$

In the above equations $\hat{x}_{k|k-1}$ is the a priori estimation and $\hat{x}_{k|k}$ is the a posteriori estimation of x_k. Also $P_{k|k-1}$ and $P_{k|k}$ are the covariance of a priori and a posteriori estimations respectively. K_k, is the optimum Kalman gain [12-15]. The Kalman Filter requires accurate knowledge of process and measurement noise covariances, but these quantities are typically unknown in real systems, often leading to estimation errors or divergence. Adaptive Kalman Filtering methods—such as forgetting-factor approaches—address this issue by updating noise covariances online to improve reliability and tracking performance.

$$P_{k|k-1} = \frac{1}{l}(F_k P_{k-1|k-1} F_k^{\phi} + Q_k) \tag{9}$$

2.2 Adaptive-R EKF

In this variant, the measurement noise covariance R_k is updates online using innovation sequence:

$$R_k = \lambda R_{k-1} + (1-\lambda)\nu_k \nu_k'$$

where $\lambda \in [0,1)$ is the forgetting factor.

2.3 Forgetting Factor EKF

This method modifies the prediction covariance to emphasize recent information:

$$P_{k|k-1} = \frac{1}{l}(F_k P_{k-1|k-1} F_k^{\phi} + Q_k)$$

All other EKF steps remain unchanged.

2.4. Mahalanobis Distance-Based EKF

This approach evaluates the consistency of each measurement using the Mahalanobis distance:

$$d_k^2 = \nu_k' S_k^{-1} \nu_k$$

Decision Rule:

If $d_k^2 > \chi_{p,\alpha}^2$: reject the measurement

Else: accept and update as in standard EKF

3.2. METHODOLOGY

This study assesses four Extended Kalman Filter (EKF) variants for real-time estimation of indocyanine green (ICG) concentration in tumor-bearing rats: the standard EKF with fixed noise parameters, the Adaptive-R EKF with time-varying measurement noise, the Forgetting Factor EKF that emphasizes recent data, and the Mahalanobis Distance EKF that suppresses outliers. Applied to real ICG pharmacokinetic data, these methods operate within a three-dimensional state-space representation that models concentration alongside its temporal derivatives, providing improved accuracy and interpretability for pharmacokinetic analysis under uncertainty.

3.3 ICG pharmacokinetic Model

The ICG pharmacokinetic data is modeled as a discrete-time dynamic system with a three-dimensional state vector. Let the state vector be defined as:

$$x_k = \begin{bmatrix} p_k \\ v_k \\ a_k \end{bmatrix}$$

where,

p_k is the ICG pharmacokinetic level at time k

v_k is the velocity (rate of change of ICG pharmacokinetic level)

a_k is the acceleration (rate of change of velocity)

$$x_k = f(x_k) + w_k$$

$$f(x_k) = [p_k + v_k + 0.5a_k, v_k + 0.5a_k, a_k]$$

is the nonlinear state transition. The state evolution is defines as:

$$x_k = F_k x_{k-1} + w_{k-1}$$

$$F = \begin{bmatrix} 1 & \Delta t & 0.5\Delta t^2 \\ 0 & 1 & \Delta t \\ 0 & 0 & 1 \end{bmatrix}$$

The observation model is:

$$y_k = H_k x_{k-1} + v_{k-1},$$

$$H = \begin{bmatrix} 1 & 0 & 0 \end{bmatrix}$$

4. RESULTS

The compartmental model was evaluated using experimental data provided by collaborators, with full details of the experimental setup available in [5]. Since this study concentrates on modeling and parameter estimation, only a brief overview of the protocol is given here to support the mathematical formulation. ICG was injected intravenously into tumor-bearing rats, and optical signals were recorded over the tumor surface. After binding to albumin, ICG normally remains in the vascular space, but tumor-induced permeability allows leakage into the EES, enabling tumor detection. These kinetics are analyzed with the compartmental model, and EKF performance is measured using RMSE, MAE, MAPE, and R^2. We evaluated each filter using ICG pharmacokinetic data, RMSE, MAE, MAPE, R^2 was computed.

Table 1. Performance Comparison

Model	**RMSE**	**MAE**	**MAPE**	R^2
Standard EKF	0.000045	0.000025	0.009327	1.000000
Adaptive-R EKF	0.000030	0.000005	0.004694	1.000000
FF EKF	0.000044	0.000024	0.008992	1.000000
Mahalanobis EKF	0.000045	0.000025	0.009327	1.000000

When Table 1 is analyzed, the best result is obtained with Adaptive-R EKF. The actual and estimated results obtained with Adaptive-R EKF, estimated speed and acceleration values are shown in Figure 1. All four EKF variants were applied to the same ICG pharmacokinetic dataset, and their performance was evaluated using RMSE. The Adaptive-R EKF achieved the lowest error (0.000030), benefiting from its innovation-driven adaptation of the measurement noise covariance. The Forgetting Factor EKF also performed competitively, particularly in capturing transient dynamics by prioritizing recent observations. The Mahalanobis EKF maintained stable performance by suppressing outliers, an important advantage when dealing with noisy biomedical data. Beyond concentration estimation, incorporating velocity and acceleration provided a richer depiction of ICG kinetics. Velocity reflects the instantaneous rate of uptake or clearance, while acceleration captures second-order transitions such as perfusion shifts or treatment-related vascular changes. These additional states enhance physiological interpretability and are especially valuable in modeling the non-stationary behavior characteristic of tumor environments.

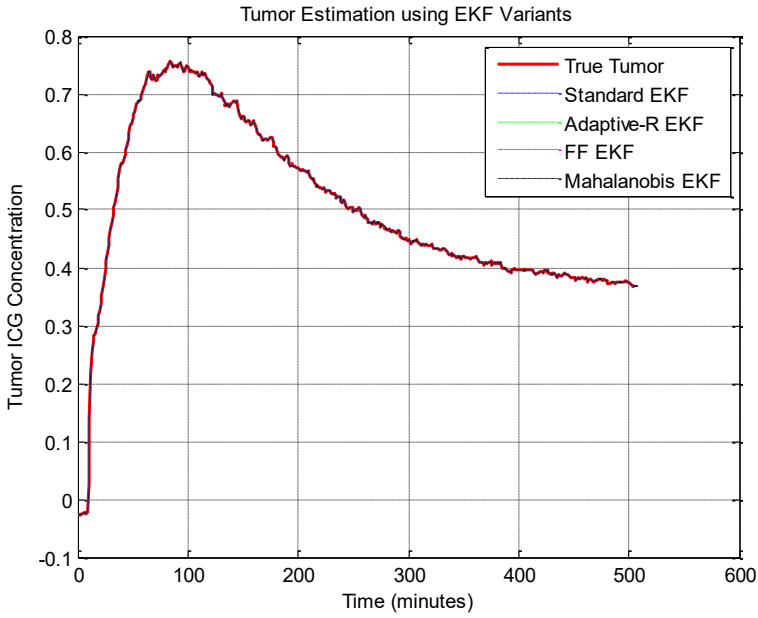

Figure 1: ICG Concentration – Adaptive-R EKF

CONCLUSION

This study demonstrates that Extended Kalman Filter variants—enhanced with velocity and acceleration states—elevate pharmacokinetic analysis from simple concentration tracking to dynamic vascular monitoring. By providing real-time, derivative-aware estimates, these EKF frameworks offer a robust foundation for characterizing tumor microenvironments and supporting precision diagnostics and therapeutic decision-making in oncology.

REFERENCES

[1] P. S. Tofts, "Modeling tracer kinetics in dynamic Gd-DTPA MR imaging," *J. Magn. Reson. Imag.*, vol. 7, pp. 91–101, 1997.

[2] M. Y. Su, J. C. Jao, and O. Nalcioglu, "Measurement of vascular volume fraction and blood-tissue permeability constants with a pharmacokinetic model: studies in rat muscle tumors with dynamic Gd-DTPA enhanced MRI," *Magn. Reson. Med.*, vol. 32, pp. 714–724, 1994.

[3] V. Ntziachristos, A. G. Yodh, M. Schnall, and B. Chance, "Concurrent MRI and diffuse optical tomography of breast after indocyanine green enhancement," *Proc. Natl. Acad. Sci. USA*, vol. 97, pp. 2767–2772, 2000.

[4] K. Botsman, K. Tickle, and J. D. Smith, "A Bayesian formulation of the Kalman filter applied to the estimation of individual pharmacokinetic parameters," *Comput. Biomed. Res.*, vol. 30, pp. 83–93, 1997.

[5] L. Özbek and M. Efe, "An adaptive extended Kalman filter with application to compartment models," *Commun. Stat. Simul. Comput.*, vol. 33, no. 1, pp. 145–158, 2004.

[6] B. Alacam, B. Yazici, and B. Chance, "Extended Kalman filtering for the modeling and analysis of ICG pharmacokinetics in cancerous tumors using NIR optical methods," *IEEE Trans. Biomed. Eng.*, vol. 53, no. 10, pp. 1861–1871, 2006, doi: 10.1109/TBME.2006.881796.

[7] B. Alacam, B. Yazici, S. Nioka, and B. Chance, "Pharmacokinetic-rate images of indocyanine green for breast tumors using near-infrared optical methods," *Phys. Med. Biol.*, vol. 53, pp. 837–859, 2008, doi: 10.1088/0031-9155/53/4/002.

[8] B. Alacam and B. Yazici, "Direct reconstruction of pharmacokinetic-rate images of optical fluorophores from NIR measurements," *IEEE Trans. Med. Imag.*, vol. 28, no. 9, pp. 1337–1353, 2009, doi: 10.1109/TMI.2009.2015294.

[9] L. Özbek, M. Efe, E. K. Babacan, and N. Yazıhan, "Online estimation of capillary permeability and contrast agent concentration in rat tumors," *Hacet. J. Math. Stat.*, vol. 39, no. 2, pp. 283–293, 2010.

[10] O. Gottam, N. Naik, and S. Gambhir, "Parameterized level-set based pharmacokinetic fluorescence optical tomography using the regularized

Gauss–Newton filter," *J. Biomed. Opt.*, vol. 24, no. 3, pp. 031010, 2019, doi: 10.1117/1.JBO.24.3.031010.

[11] O. Gottam, N. Naik, S. Gambhir, and P. K. Pandey, "RBF level-set based fully-nonlinear fluorescence photoacoustic pharmacokinetic tomography," *Inverse Probl. Sci. Eng.*, 2021, doi: 10.1080/17415977.2021.1982934.

[12] F. Aliev and L. Özbek, "Evaluation of convergence rate in the central limit theorem for the Kalman filter," *IEEE Trans. Autom. Control*, vol. 44, no. 10, pp. 1905–1909, 1999.

[13] R. E. Kalman, "A new approach to linear filtering and prediction problems," *J. Basic Eng.*, vol. 82, pp. 35–45, 1960.

[14] B. D. O. Anderson and J. B. Moore, *Optimal Filtering*. Englewood Cliffs, NJ, USA: Prentice Hall, 1979.

[15] A. H. Jazwinski, *Stochastic Processes and Filtering Theory*. New York, NY, USA: Academic Press, 1970.

CHAPTER 4

DYNAMIC GROWTH MODELING OF ADANA DEWLAP PIGEONS USING ADAPTIVE LOCAL LEVEL TREND KALMAN FILTERING

Assoc. Prof. Dr. Levent ÖZBEK[1]

DOI: https://www.doi.org/10.5281/zenodo.18077849

[1] Ankara University, Faculty of Science, Department of Statistics, Ankara, Türkiye. ozbek@science.ankara.edu.tr, orcid id:000-0003-1018-3114

1. INTRODUCTION

Throughout human civilization, pigeons have served roles far beyond their modest appearance—ranging from symbolic figures of peace to reliable couriers. Originating from the wild rock pigeon (*Columba livia*), centuries of selective breeding have produced numerous varieties with striking morphological diversity [1–3]. Among these, the Adana Dewlap pigeon—traditionally bred in the southern regions of Türkiye—distinguishes itself with its characteristic bone structure, pronounced dewlap, and recognizable flight behavior. Despite its cultural relevance and genetic uniqueness, scientific information regarding its developmental patterns and growth trajectory remains limited.

Understanding how birds grow is crucial not only for biological insight but also for improving breeding efficiency and flock management. Classical sigmoidal growth models—such as the Gompertz, Logistic, and Richards equations—are widely applied to describe body-weight changes over time. Although these models often represent the general shape of growth curves satisfactorily, they fall short when rapid fluctuations occur due to biological noise, environmental variation, or irregular measurement intervals. To overcome these constraints, the present study incorporates both traditional nonlinear functions and a dynamic state-space methodology via the Kalman Filter (KF) and Adaptive Kalman Filter (AKF). Logistic, Richards, and Gompertz models were first applied to a 43-day longitudinal dataset obtained from 88 Adana Dewlap pigeons. Their performance was assessed using standard accuracy indicators: Mean Squared Error (MSE), Mean Absolute Percentage Error (MAPE), and coefficient of determination (R^2).

The state-space approach allows KF to estimate hidden components of the growth process—such as instantaneous body weight, rate of change, and acceleration—while AKF adjusts the process noise parameters in response to abrupt biological shifts. This dual framework effectively captures both the rapid early growth phase and the slowdown observed later in development, offering advantages over fixed-parameter curve fitting. Consequently, integrating nonlinear growth equations with adaptive filtering provides a versatile analytical tool for real-time monitoring, identifying anomalies, and supporting management decisions in pigeon breeding.

Earlier research in poultry growth modeling has highlighted the suitability of Gompertz and Richards structures due to their biological interpretability [4–5]. Building on this foundation, Özbek (2022, 2023) evaluated multiple growth functions using body-weight measurements from Adana Dewlap pigeons and concluded that the Richards model yielded the most accurate static representation [6–8]. In subsequent work, coupling a Discrete-Time Stochastic Gompertz formulation with AKF enabled online tracking of time-dependent parameters and displayed strong predictive performance (MSE ≈ 270; $R^2 \approx 0.98$; MAPE $\approx 2.3\%$) [8].

Environmental conditions exert a significant influence on reproductive timing. In colder seasons, the incubation period typically lasts around 45 days, whereas in warmer months it shortens to approximately 30–32 days due to improved thermal conditions [9–10]. Pigeon hatchlings are altricial and depend completely on parental care. Their initial survival is shaped primarily by:

(i) the nutrient-rich crop milk supplied by the parents, and

(ii) warmth provided through continuous brooding.

Maternal body mass indirectly reflects nutritional reserves and crop-milk production capacity; heavier and well-nourished females are generally more efficient in supporting chick development [11–16].

2. MATERIALS AND METHODS

2.1. State-space model representation for pigeon growth

In the 1960s, linear discrete-time stochastic state-space models were developed for applications such as tracking and controlling the position of satellites, guided missiles, spacecraft, and maneuvering targets. In addition to these aerospace applications, the state-space modeling approach has also found widespread use in modeling physical, physiological, and economic processes [17–20]. The problem of estimating the state vector within a linear discrete-time stochastic state-space framework was first introduced by Kalman [21]. The Kalman Filter (KF) can essentially be defined as a recursive solution to the least-squares estimation problem [22–24]. There is an extensive body of literature on the derivation of the Kalman filter, its theoretical properties, and its applications across different scientific fields [25–28].

2.2. Model Structure

The LLT model describes the evolution of the growth process as:
State Equation:

$$x_{k+1} = F_k x_k + w_k \quad (1)$$

Observation Equation:

$$y_k = H_k x_k + v_k \quad (2)$$

$$F_k = \begin{bmatrix} 1 & \Delta_t \\ 0 & 1 \end{bmatrix},\ H_k = [1, 0]$$

where $x_k = [level,\ slope]^T$ and $w_k \sim N(0, Q)$, $v_k \sim N(0, R)$. Process and measurement covariances were defined as $Q_k = diag(q_l, q_b)$ and R = r.

2.3. Adaptive Noise Tuning

Measurement noise R was initialized robustly using median absolute deviation (MAD):

$$r_0 = (1.4826 x MAD(y))^2$$

Normalized Innovation Squared (NIS):

$$NIS_k = \frac{v_k^2}{S_k}$$

$$S_k = HP_k H_k^T + R$$

Adaptive update of R and ql followed a smoothed rule:

$$r_{k+1} = r_k \left(\frac{\overline{NIS}_w}{1.0} \right)^{0.5}$$

where $\overline{NIS}_w$ is the moving average over a window of size W = 50. Covariance updates were performed in Joseph form:

$$P_k = (I - K_k H) P_k (K_k H)^T + K_k R K_k^T$$

2.4. Performance Metrics

Mean Squared Error (MSE): The MSE measures the square root of the average of the squared differences between the predicted and actual values. It penalizes larger errors more heavily than smaller ones:

$$MSE = \frac{1}{n} \sum_{i=1}^{n} (y_i - \hat{y}_i)^2$$

where y_i is the actual value, $\hat{y}_i$ is the predicted value, and *n* is the total number of observations.

Mean Absolute Percentage Error (MAPE): MAPE expresses prediction accuracy as a percentage, making it scale-independent. However, it becomes undefined when any actual value y_i equals zero:

$$MAPE = \frac{100\%}{n} \sum_{i=1}^{n} \left| \frac{y_i - \hat{y}_i}{y_i} \right|$$

Coefficient of Determination (R^2): R^2 represents the proportion of the variance in the dependent variable that is predictable from the independent variables. It is calculated as:

$$R^2 = 1 - \frac{\sum_{i=1}^{n} (y_i - \hat{y}_i)^2}{\sum_{i=1}^{n} (y_i - \bar{y}_i)^2}$$

where $\overline{y}$ is the mean of the actual values.

3. RESULTS AND DISCUSSION

The adaptive LLT-Kalman filter converged stably after six iterations with consistent NIS near unity. Table 1 compares its performance against conventional models.

Table 1: Comparison of growth model performance on Adana Dewlap pigeon data.

Model	**MSE**	**MAPE (%)**	**R^2**	**AIC**
Logistic	68.24	3.52	0.9910	-225.4
Gompertz	57.11	2.95	0.9932	-237.9
Richards	53.87	2.64	0.9941	-241.5
LLT–Kalman	49.42	2.08	0.9975	-50.8

The LLT-Kalman model achieved the lowest MSE and highest R^2, indicating excellent fit and predictive precision. Fig. 1 shows the observed and estimated trajectories with 95% confidence limits, while Fig. 2 and Fig. 3 present the slope and NIS evolution, respectively.

4. CONCLUSION

The Adaptive LLT-Kalman framework provides a powerful, data-driven approach for modeling dynamic biological growth processes. It adaptively captures local deviations, stabilizes estimation under measurement noise, and yields higher accuracy than conventional parametric models. This study highlights the potential of recursive Kalman-based models for advanced growth analysis in avian species.

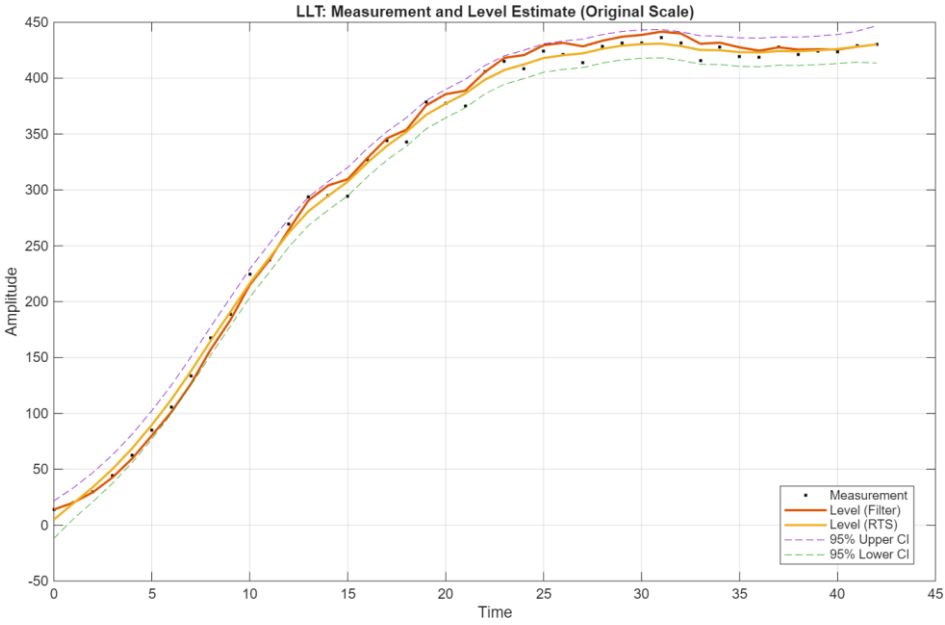

Figure 1: LLT–Kalman estimation of growth curve.

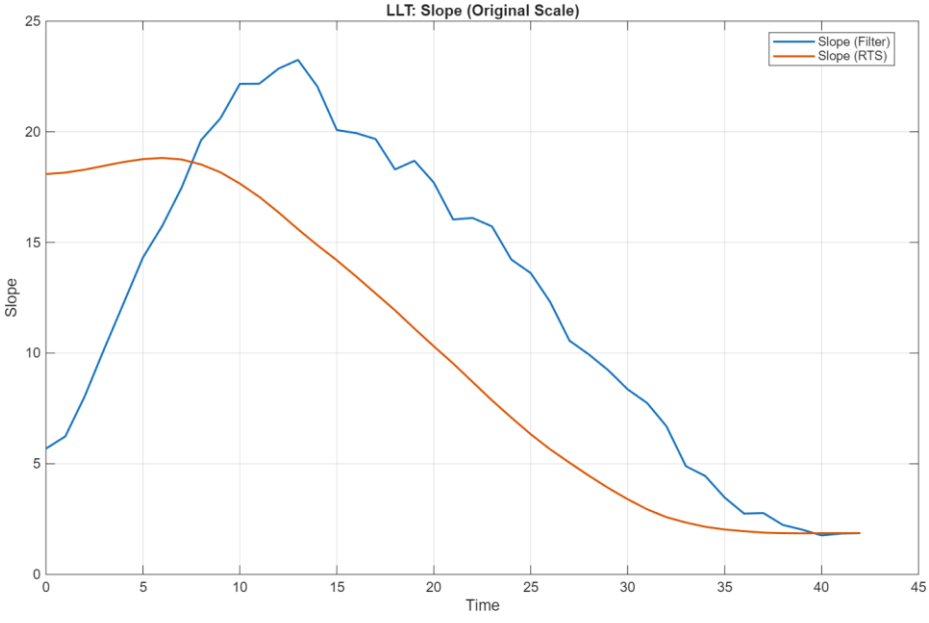

Figure 2: Trend (slope) component.

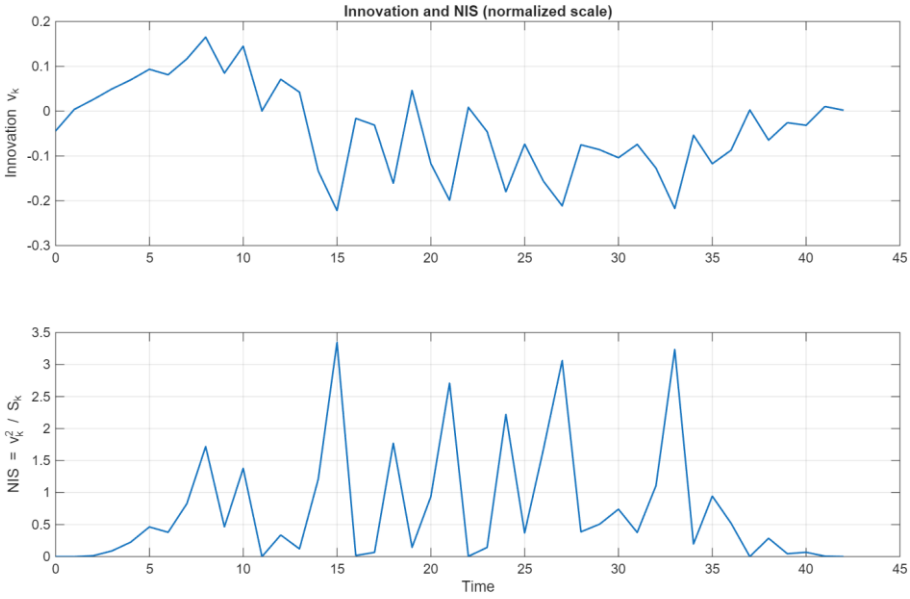

Figure 3: Innovation and NIS.

REFERENCES

1. Shapiro M. Genomic diversity and evolution of the head crest in the rock pigeon. Science. 2013;339(6123):1063–1067.
2. Yılmaz O, Ertuğrul M. Importance of pigeon husbandry in history. J Harran Univ Agric. 2012;16(2):1–7.
3. Secord JA. Charles Darwin and the breeding of pigeons. Nature's Fancy. 1981;72(2):162–186.
4. Narinç D, et al. Growth curve analyses in poultry science. World's Poult Sci J. 2017;73(2):395–408.
5. Darmani Kuhi H, et al. A review of mathematical functions for growth in poultry. World's Poult Sci J. 2010;66(2):227–240.
6. Özbek L. Modeling growth of Adana pigeons. Comm Fac Sci Univ Ank A2-A3. 2022;64(2):95–103.
7. Özbek L. Discrete-Time Gompertz Model for Adana Breed Pigeons. GU J Sci. 2023;36(3):1382–1390.
8. Özbek L. Adana Dewlap Pigeons and Statistical Growth Models. Braz J Poult Sci. 2024;26(4):1–6.
9. Johnston RF, Janiga M. Feral Pigeons. Oxford Univ Press; 1995.
10. Levi WM. The Pigeon. Levi Publ; 1977.
11. Goldstein DL, Flake RE. Composition of pigeon crop milk. The Auk. 1971;88(1):119–122.
12. Gillespie MJ, et al. Pigeon 'milk' and mammalian milk similarities. PLoS ONE. 2014;9(3):e92424.
13. Shetty S, et al. Avian crop milk. Int J Vet Sci. 2019;8(1):1–6.
14. Gompertz B. Law of human mortality. Philos Trans R Soc Lond. 1825;115:513–583.
15. Richards FA. A flexible growth function. J Exp Bot. 1959;10:290–300.
16. Tjørve KM, Tjørve E. Use of Gompertz models. PLoS ONE. 2017;12(6):e0178691.
17. Ozbek L, Ozlale U. Extended Kalman filter for output gap. J Econ Dyn Control. 2005;29(9):1611–1622.
18. Özbek L, et al. Motor unit pattern decomposition via Kalman filter. GU J Sci. 2010;23(2):155–162.

19. Ozbek L, Efe M. Adaptive EKF with compartment models. Commun Stat Simul Comput. 2004;33(1):145–158.
20. Özbek L. AKF for nonlinear gene networks. Comm Fac Sci Univ Ank A1. 2020;69(2):211–220.
21. Kalman RE. Linear Filtering and Prediction. J Basic Eng. 1960;82:35–45.
22. Diderrich GT. Kalman filter and Theil estimators. Am Stat. 1985;39:193–198.
23. Duncan DB, Horn SD. Recursive estimation. JASA. 1971;67:815–821.
24. Meinhold RJ, Singpurwalla ND. Understanding Kalman filter. Am Stat. 1983;84:479–486.
25. Jazwinski AH. Stochastic Processes and Filtering Theory. Acad Press; 1970.
26. Anderson BDO, Moore JB. Optimal Filtering. Prentice Hall; 1979.
27. Chen G. Approximate Kalman Filtering. World Scientific; 1993.
28. Özbek L, Aliev FA. Adaptive fading Kalman filter. Automatica. 1998;34(12):1663–1664.

CHAPTER 5

THE HADAMARD-TYPE PELL-p SEQUENCE IN FINITE GROUPS

Assoc. Prof. Dr. Yeşim AKÜZÜM ÖZEN [1]

DOI: https://www.doi.org/10.5281/zenodo.18077958

[1]Kafkas University, Faculty of Science and Letters, Department of Mathematics, Kars,Türkiye, E-mail: ysmakuzum89@gmail.com, Orcid.: 0000-0001-7168-84

INTRODUCTION

The investigation of recurrence sequences within algebraic structures has its origins in the foundational work of Wall (Wall, 1960), who examined the behavior of the classical Fibonacci sequence in the context of cyclic groups. Wall's study demonstrated how fundamental number-theoretic recurrences could interact with group operations, thereby initiating a new line of inquiry that connected recurrence relations with algebraic systems.

Building on this early foundation, Wilcox (Wilcox, 1986) broadened the scope of the theory by extending the study from cyclic groups to general abelian groups. His work provided a systematic framework for understanding how recurrence sequences, originally defined over the integers, could be adapted to operate within more complex algebraic environments. This extension played a significant role in shaping subsequent research on recurrence sequences in various group-theoretic settings.

Later, Lü and Wang (Lü & Wang, 2007) contributed to this line of research by examining Wall numbers associated with the k-step Fibonacci sequence. Their work extended the classical notion of Wall numbers-which originally arose in the study of ordinary Fibonacci recurrences-to higher-order recurrence relations. By generalizing the concept to k-step sequences, they provided new insights into the periodic behavior and structural properties of these sequences modulo m, thereby enriching the theory of recurrence sequences in algebraic and number-theoretic settings.

In another significant development, Knox (Knox, 1992) introduced the k-nacci sequence by interpreting the k-step Fibonacci recurrence within groups and conducted a detailed analysis of its properties in finite groups. Together, these studies highlight the rich interplay between recurrence relations and group structures and form an essential foundation for subsequent investigations in this area.

In the subsequent developments, the theory was further extended to the generalized order-k Pell sequence by Deveci and Karaduman (Deveci & Karaduman, 2015), who formulated the order-k Pell recurrence in an algebraic framework and examined its structural and periodic properties. Their work broadened the classical recurrence theory by incorporating higher-order Pell-type relations, thus enriching the understanding of generalized recurrence sequences within algebraic and number-theoretic contexts.

In recent years, a variety of linear recurrence sequences constructed using group elements have been the subject of extensive study; for example, (Aydin & Dikici, 1998; Campbell & Campbell, 2004; Deveci, Akuzum, Karaduman, & Erdag, 2015; Deveci, Erdag, & Gungoz, 2023; Deveci & Karaduman, 2015; Deveci, Karaduman, & Campbell, 2011) (Doostie & Hashemi, 2006; Erdag, 2024; Erdag & Deveci, 2022; Erdag, Deveci, & Karaduman, 2022; Erdag, Halıcı, & Deveci , 2022; Erdag, Shannon, & Deveci, 2018) (Hashemi & Mehraban, 2022; Hulku, Erdag, & Deveci, 2023; Ozkan, 2007; Ozkan, Aydin, & Dikici, 2003)

In this study, we extend the Hadamard-type Pell-*p* sequence to groups by redefining it in terms of group elements, and we refer to the resulting structure as the Hadamard-type Pell-*p* orbit. Furthermore, as an application of the general results obtained, we determine the periods of the Hadamard-type Pell-3 orbit on the semidihedral groups SD_{2^m}

1. PRELIMINARIES

In the study of Akuzum, Deveci and Incekara (Akuzum, Deveci, & Incekara , is submitted), the Hadamard-type Pell-*p* sequence is introduced through the following homogeneous linear recurrence relation for $n \geq 0$ and $p \geq 3$

$$a_{n+p+1}^{p} = 2a_{n+p}^{p} - a_{n+2}^{p} + 2a_{n+1}^{p} - a_{n}^{p}$$

in which $a_0^p = a_1^p = \cdots = a_{p-1}^p = 0$ and $a_p^p = 1$.

Also, in Akuzum, Deveci and Incekara (Akuzum, Deveci, & Incekara , is submitted), the authors presented the Hadamard-type Pell-*p* matrix as follows:

$$G_p = \begin{bmatrix} 2 & 0 & \cdots & 0 & -1 & 2 & -1 \\ 1 & 0 & 0 & \cdots & 0 & 0 & 0 \\ 0 & 1 & 0 & 0 & \cdots & 0 & 0 \\ 0 & 0 & 1 & 0 & 0 & \cdots & 0 \\ \vdots & \ddots & \ddots & \ddots & \ddots & \ddots & \vdots \\ 0 & \cdots & 0 & 0 & 1 & 0 & 0 \\ 0 & 0 & \cdots & 0 & 0 & 1 & 0 \end{bmatrix}_{(p+1)\times(p+1)}$$

In addition, for $n \geq p$, they established that

$$(G_p)^n = \begin{pmatrix} a_{n+p}^p & & 2a_{n+p-1}^p - a_{n+p-2}^p & -a_{n+p-1}^p \\ a_{n+p-1}^p & & 2a_{n+p-2}^p - a_{n+p-3}^p & -a_{n+p-2}^p \\ \vdots & G_p^* & \vdots & \vdots \\ a_{n+1}^p & & 2a_n^p - a_{n-1}^p & -a_n^p \\ a_n^p & & 2a_{n-1}^p - a_{n-2}^p & -a_{n-1}^p \end{pmatrix}.$$

where G_p^* is a $(p+1)\times(p-2)$ matrix as follows:

$$\begin{bmatrix} -a_{n+2}^p + 2a_{n+1}^p - a_n^p & -a_{n+3}^p + 2a_{n+2}^p - a_{n+1}^p & \cdots & -a_{n+p-1}^p + 2a_{n+p-2}^p - a_{n+p-3}^p \\ -a_{n+1}^p + 2a_n^p - a_{n-1}^p & -a_{n+2}^p + 2a_{n+1}^p - a_n^p & \cdots & -a_{n+p-2}^p + 2a_{n+p-3}^p - a_{n+p-4}^p \\ \vdots & \vdots & \ddots & \vdots \\ -a_{n-p+3}^p + 2a_{n-p+2}^p - a_{n-p+1}^p & -a_{n-p+4}^p + 2a_{n-p+3}^p - a_{n-p+2}^p & \cdots & -a_n^p + 2a_{n-1}^p - a_{n-2}^p \\ -a_{n-p+2}^p + 2a_{n-p+1}^p - a_{n-p}^p & -a_{n-p+3}^p + 2a_{n-p+2}^p - a_{n-p+1}^p & \cdots & -a_{n-1}^p + 2a_{n-2}^p - a_{n-3}^p \end{bmatrix}.$$

It should be noted that $\det G_p = (-1)^{p+1}$.

Definition 1. The semidihedral group SD_{2^m}, ($m \geq 4$) is defined by the presentation

$$SD_{2^m} = \left\langle x, y : x^{2^{m-1}} = y^2 = e,\ yxy = x^{2^{m-2}-1} \right\rangle$$

Note that $\left|SD_{2^m}\right| = 2^m$, $|x| = 2^{m-1}$ and $|y| = 2$.

Definition 2. A sequence is periodic when, after some index, it repeats a specific block of terms. The length of the smallest block that repeats is defined as the period. Specifically, if the initial k terms of the sequence form the repeating block, then the sequence is said to be simply periodic with period k.

2. MAIN RESULTS

Let G be a finite j-generator group and let

$$X=\left\{\left(x_0,x_1,\ldots,x_{j-1}\right)\in\underbrace{G\times G\times\cdots\times G}_{j}\;\middle|\;\left\langle\left\{x_0,x_1,\ldots,x_{j-1}\right\}\right\rangle=G\right\}.$$

We call $\left(x_0,x_1,\ldots,x_{j-1}\right)$ a generating j-tuple for G.

Definition 3. For a generating j-tuple $\left(x_0,x_1,\ldots,x_{j-1}\right)\in X$, We define the Hadamard-type Pell-p orbit $q^p\left(G:x_0,x_1,\ldots,x_{j-1}\right)$ by the following expression:

$$q^p\left(n+p+1\right)=\left(q^p\left(n\right)\right)^{-1}\left(q^p\left(n+1\right)\right)^2\left(q^p\left(n+2\right)\right)^{-1}\left(q^p\left(n+p\right)\right)^2$$

for $n\geq 0$, with initial conditions

$$\begin{cases}q^p\left(0\right)=x_0,q^p\left(1\right)=x_1,\ldots,q^p\left(j-1\right)=x_{j-1},q^p\left(j\right)=e,\ldots,q^p\left(p\right)=e & \text{if } j<p,\\ q^p\left(0\right)=x_0,q^p\left(1\right)=x_1,q^p\left(2\right)=x_2,q^p\left(3\right)=x_3,\ldots,q^p\left(p\right)=x_p & \text{if } j=p.\end{cases}$$

Theorem 1. For a finite group G, the Hadamard-type Pell-p orbit orbit is simply periodic. Thus, it is easy to see that at least one of the 5-tuples occurs twice in the Hadamard-type Pell-p orbit. Because a 5-tuple appears more than once, the Hadamard-type Pell-p orbit of the group G is periodic. As the orbit $q^p\left(G:x_0,x_1,\ldots,x_{j-1}\right)$ is periodic, there exist natural number h and f with $h\equiv f\left(\mathrm{mod}\,4\right)$, such that

$$q^p\left(h\right)=q^p\left(f\right),q^p\left(h+1\right)=q^p\left(f+1\right),,\ldots,q^p\left(h+3\right)=q^p\left(f+3\right),.$$

From the definition of the Hadamard-type Pell-p orbit $q^p\left(G:x_0,x_1,\ldots,x_{j-1}\right)$, we obtain that

$$\left(q^p\left(n\right)\right)^{-1}=\left(q^p\left(n+1\right)\right)^2\left(q^p\left(n+2\right)\right)^{-1}\left(q^p\left(n+p\right)\right)^2q^p\left(n+p+1\right)^{-1}.$$

Therefore, we obtain $q^p\left(h\right)=q^p\left(f\right)$, and consequently

$$q^p(h-f)=q^p(0), q^p(h-f+1)=q^p(1),\ldots,q^p(h-f+3)=q^p(3)$$

which shows that the Hadamard-type Pell-*p* orbit is simply periodic.

We denote the length of the period of Hadamard-type Pell-*p* orbit $q^p\left(G:x_0,x_1,\ldots,x_{j-1}\right)$ by the symbol $Lq^p\left(G:x_0,x_1,\ldots,x_{j-1}\right)$.

We now provide the period lengths of the Hadamard-type Pell-3 orbit of the semidihedral group SD_{2^m}, as applications of the results established above.

Theorem 2. The length of the period of the Hadamard-type Pell-3 orbit of the semidihedral group SD_{2^m} is $3\cdot 2^{m-2}$.

Proof. The result is proved by direct computation. The orbit $q^p\left(SD_{2^m}:x,y\right)$ is

$$x, y, e, e, x^{-1}, x^2y, x, x^{-2}y, e, x^2, x^3,$$
$$x^{-6}y, x, x^{-4}y, x^{-4}, x^4, x^{-5}, x^2y, x,$$
$$x^2y, x^4, x^6, x^7, x^2y, x, x^8y, x^8, x^8, \ldots.$$

From the above results, it follows that the orbit has the following form:

$$q^p(0)=x,\ q^p(1)=y,\ q^p(2)=e,\ q^p(3)=e\ldots,$$
$$q^p(12i)=x,\ q^p(12i+1)=x^{4i.k_1}y,\ q^p(12i+2)=x^{4i.k_2}, q^p(12i+3)=x^{4i.k_3},\ \ldots.$$

Where k_1, k_2 and k_3 are positive integers satisfying $\gcd(k_1,k_2,k_3)=1$. Thus, for $\alpha\in N$, we need the smallest integer i such that $4i=2^{m-1}\cdot\alpha$. If we take $i=2^{m-3}$, we obtain

$$q^p\left(12.2^{m-3}\right)=x,\ q^p\left(12.2^{m-3}+1\right)=y,$$
$$q^p\left(12.2^{m-3}+2\right)=e,\ q^p\left(12.2^{m-3}+3\right)=e,\ \ldots.$$

Because the next elements depend on x, y and e, the cycle restarts at the $\left(12.2^{m-3}\right)$-th term. Thus, it is confirmed that the period length of the Hadamard-type Pell-3 orbit of the semidihedral group SD_{2^m} is $3\cdot 2^{m-2}$.

Example 1. The orbit $q^p\left(SD_{16}:x,y\right)$ is

$$x,y,e,e,x^{-1},x^2y,x,x^6y,e,x^2,x^3,$$
$$x^2y,x,x^4y,x^4,x^4,x^3,x^2y,x,$$
$$x^2y,x^4,x^6,x^7,x^2y,x,y,e,e,\ldots.$$

So we obtain that $Lq^p\left(SD_{16}:x,y\right)=24$.

CONCLUSION

In this study, we extend the Hadamard-type Pell-*p* sequence to groups by redefining it through group elements and introducing the Hadamard-type Pell-*p* orbit. We prove that this orbit is simply periodic for any finite group. As an application, we analyze the Hadamard-type Pell-3 orbit on the semidihedral groups SD_{2^m} and determine the lengths of its periods by using the general results obtained.

REFERENCES

Akuzum, Y., Deveci, O., & Incekara , A. (is submitted). The Hadamard-type Pell-p Sequences.

Aydin, H., & Dikici, R. (1998). General Fibonacci Sequences in Finite Groups. *Fibonacci Quarterly, 36*(3), 216-221.

Campbell, C., & Campbell, P. (2004). *On the Fibonacci length of powers of dihedral groups. In Applications of Fibonacci numbers,* (Cilt 9). Dordrecht, The Netherlands.: F. T. Howard, Ed., Kluwer Academic Publisher.

Deveci, O., & Karaduman, E. (2015). The Pell Sequences in Finite Groups. *Utilitas Mathematica, 96*, 263-276.

Deveci, O., Akuzum, Y., Karaduman, E., & Erdag, O. (2015). The Cyclic Groups via Bezout Matrices. *Journal of Mathematics Research, 7*(2), 34-41.

Deveci, O., Erdag, O., & Gungoz, U. (2023). The complex-type cyclic-Fibonacci sequence and its applications. *Journal of Mahani Mathematical Research, 12*(2), 235-246.

Deveci, O., Karaduman, E., & Campbell, C. (2011). On the k-nacci sequences in finite binary polyhedral groups. *Algebra Colloq., 18*(1), 945-954.

Doostie, H., & Hashemi, M. (2006). Fibonacci lengths involving the Wall number k(n). *Journal of Applied Mathematics and Computing, 20*(1), 171-180.

Erdag, O. (2024). The Narayana-Pell Sequence in Finite Groups. İ. Eryılmaz içinde, *Unified Perspectives in Mathematics and Geometry* (s. 163-174). Ankara: BIDGE Publications.

Erdag, O., & Deveci, O. (2022). On the Connections between Padovan Numbers and Fibonacci p-Numbers. *Jordan Journal of Mathematics and Statistics, 15*(3), 507-521.

Erdag, O., Deveci, O., & Karaduman, E. (2022). The complex-type cyclic-Pell sequence and its applications. *Turkish Journal of Science, 7*(3), 202-210.

Erdag, O., Halıcı, S., & Deveci , O. (2022). The complex-type Padovan-p sequences. *Mathematica Moravica, 26*(1), 77-88.

Erdag, O., Shannon, A., & Deveci, O. (2018). The arrowhead-Pell-Random-type sequences. *Notes Number Theory Discrete Mathematics, 24*(1), 109-119.

Hashemi, M., & Mehraban, E. (2022). The generalized order k-Pell sequences in some special groups of nilpotency class 2. *Communications in Algebra, 54*(2), 1768-1784.

Hulku, S., Erdag, O., & Deveci, O. (2023). Complex-type Narayana sequence and its application. *Maejo International Journal of Science & Technology, 17*(02), 163-176.

Knox, S. (1992). Fibonacci Sequences in Finite Groups. *Fibonacci Quarterly, 30*, 116-120.

Lü, K., & Wang, J. (2007). k-step Fibonacci Sequence Modulo m. *Utilitas Mathematica, 71*, 169-178.

Ozkan, E. (2007). On truncated Fibonacci sequences. *Indian Journal of Pure and Applied Mathematics, 38*(4), 241-251.

Ozkan, E., Aydin, H., & Dikici, R. (2003). 3-step Fibonacci series modulo m. *Applied Mathematics and Computation, 143*, 165-172.

Wall, D. D. (1960). Fibonacci series modulo m. *The American Mathematical Monthly, 67*, 525-532.

Wilcox, H. (1986). Fibonacci Sequences of Period n in Groups. *Fibonacci Quart, 24*(4), 356-361.

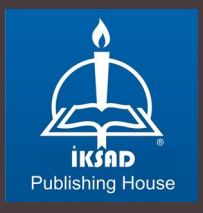

ISBN: 978-625-378-456-0